JGR Space Physics

RESEARCH ARTICLE
10.1029/2021JA030086

Key Points:

- Magnetic waves were measured by Voyagers 1 and 2 in the solar wind near the magnetosphere of Jupiter
- These waves have signatures of excitation by local pickup H^+ ions
- A neutral H loss rate of $\sim 5 \times 10^{28}$ s^{-1} from the Jovian system is estimated

Correspondence to:
C. W. Smith,
Charles.Smith@unh.edu

Citation:
Hollick, S. J., Smith, C. W., Pine, Z. B., Argall, M. R., Joyce, C. J., Isenberg, P. A., et al. (2022). Magnetic waves excited by newborn pickup H^+ near Jupiter: Neutral hydrogen loss by the planetary system. *Journal of Geophysical Research: Space Physics*, *127*, e2021JA030086. https://doi.org/10.1029/2021JA030086

Received 27 OCT 2021
Accepted 5 JUL 2022

Magnetic Waves Excited by Newborn Pickup H^+ Near Jupiter: Neutral Hydrogen Loss by the Planetary System

Sophia J. Hollick[1,2], Charles W. Smith[1], Zackary B. Pine[1,3], Matthew R. Argall[1], Colin J. Joyce[1], Philip A. Isenberg[1], Bernard J. Vasquez[1], Nathan A. Schwadron[1], Justyna M. Sokół[4], Maciej Bzowski[5], Marzena A. Kubiak[5], F. Bagenal[6], and John D. Richardson[7]

[1]Space Science Center, Morse Hall, University of New Hampshire, Durham, NH, USA, [2]Department of Physics, Yale University, New Haven, CT, USA, [3]Department of Physics and Astronomy, University of California Los Angeles, Los Angeles, CA, USA, [4]Southwest Research Institute, San Antonio, TX, USA, [5]Space Research Centre of the Polish Academy of Sciences (CBK PAN), Warsaw, Poland, [6]Laboratory for Atmospheric and Space Physics, University of Colorado Boulder, Boulder, CO, USA, [7]Kavli Center for Astrophysics and Space Science, Massachusetts Institute of Technology, Cambridge, MA, USA

Abstract We report here observations of magnetic waves recorded by the Voyager spacecraft in the solar wind near Jupiter that are possibly the result of excitation by newborn pickup H^+. Consideration of growth rates due to the known interstellar ion sources strongly disfavor an interstellar source. To determine the likely source of the waves, we compute the minimum ion production rate by equating wave growth to turbulent cascade rates and derive a lower limit for the production of H^+ at the times of observations. The only available source of neutral H at these times and at the levels required is the Jovian system, most notably charge exchange between energetic protons and the neutral clouds around Io and Europa's orbits. Further refinement of the source identity is not possible at this time. We provide an estimate for the neutral H source subject to assumptions of the latitudinal extent of the population which is not constrained by observation.

Plain Language Summary The Voyager spacecraft instruments include a fluxgate magnetometer called MAG that measures the changing ambient magnetic field. We report observations by MAG of low-frequency waves in the solar wind outside the Jovian magnetosphere that are seen at frequencies and with characteristics that suggest the waves are excited by protons that originate as neutral hydrogen. Collision with solar wind protons ionize the neutral hydrogen to produce an energetic ion population called pickup ions. We use known characteristics of wave excitation by pickup ions to estimate the rate of pickup ion production. The only source that is strong enough to produce the pickup ions with the number density required is the Jovian system.

1. Introduction

Our recent study of magnetic field data recorded by the Voyagers 1 and 2 spacecraft from launch in late 1977 through 1990 revealed 637 instances of low-frequency waves in the range of heliocentric distance $1 < R_{AU} < 45$ AU that could be readily explained as arising from newborn interstellar pickup ions (PUIs) He^+ and H^+ (Hollick et al., 2018a, 2018b, 2018c). However, that same study also revealed instances of waves close to Jupiter that appear to result from pickup H^+, but that could not be explained by an interstellar source. In the analysis of waves due to interstellar PUIs, we compared the rate of wave growth due to the scattering of newborn interstellar PUIs (Lee & Ip, 1987) to the rate of the turbulent energy cascade. The nonlinear dynamics of turbulence absorbs the wave energy and distributes it through the spectrum, thereby rendering the excited wave energy unobservable as waves due to PUIs. We found numerous examples within 75 days of closest approach to Jupiter where the ion production rate required to produce wave growth in excess of the background turbulence rate was a factor of 10× to 500× the level that could be justified by current models of the interstellar neutral inflow. Since that same theory succeeded in accounting for the wave observations due to newborn interstellar PUIs elsewhere, we concluded that these waves seen relatively close to the planet must arise from a planetary source. While we initially suspected involvement by the Jovian bow shock, we now believe that loss of neutral Hydrogen (H) by the planetary system (atmosphere, magnetosphere, satellites, dust, etc.) produces a neutral H cloud in the solar wind that is subsequently ionized by the same collision-dominated processes that produce interstellar PUIs. These

wave observations were excluded from the earlier papers describing waves due to interstellar pickup ions (Hollick et al., 2018a, 2018b, 2018c). We now turn to study these events in this paper.

Transverse, low-frequency magnetic waves that are excited by newborn pickup ions have established characteristics: they are primarily Sunward propagating and right-hand polarized in the plasma frame, but they are seen as left-hand polarized in the spacecraft frame and only at Doppler-shifted spacecraft-frame frequencies greater than the ion cyclotron frequency. Waves at lower frequencies can only be excited by a population of more energetic ions which is argued to be minimal for the interstellar source in the absence of shocks. Although left-hand polarized wave observations are expected to define the observations, we have found a large number of right-hand polarized waves that match the expectations in all other regards in the ACE, Ulysses and Voyager magnetic field data (Aggarwal et al., 2016; Cannon, Smith, Isenberg, Vasquez, Murphy, & Nuno, 2014; Fisher et al., 2016; Hollick et al., 2018a; Marchuk et al., 2021). While this suggests a modified scattering process and possibly a non-isotropic distribution of PUIs for reasons that remain unknown, they continue to be identified as waves due to newborn PUIs.

The observability of waves due to newborn interstellar PUIs is argued to depend on whether or not the energy growth rate of the wave exceeds the background turbulent energy cascade rate (Aggarwal et al., 2016; Argall et al., 2017; Cannon, Smith, Isenberg, Vasquez, Joyce, et al., 2014; Fisher et al., 2016; Hollick et al., 2018b; Joyce et al., 2010; Marchuk et al., 2021). Wave excitation is always present to the degree that ion production from neutral atoms is ongoing, but if the turbulence is sufficiently strong the wave energy will not accumulate within the unstable wavenumber range to reach observable levels. Observability does not appear to depend to a sensitive degree upon local variation of ion production, although we do take this variation into account both here and elsewhere (Hollick et al., 2018b; Marchuk et al., 2021). The turbulence levels vary to a greater degree than the local ionization dynamics. We have argued that observable spectal enhancements are not seen under average circumstances since the turbulent cascade transports the wave energy faster than it can accumulate. When the waves are not observed, it is argued that the energy excited by the PUI process enhances the background turbulence. Beyond ~10 AU, wave excitation by interstellar PUIs becomes the dominant energy source to drive the turbulence and heat the thermal plasma (Adhikari et al., 2015a, 2015b, 2017; Breech et al., 2005, 2008, 2009, 2010; Isenberg, 2005; Isenberg et al., 2003, 2010; Matthaeus et al., 1994; Ng et al., 2010; Oughton et al., 2006, 2011; Richardson & Smith, 2003; Richardson et al., 1995, 1996; Smith et al., 2001, 2006; Usmanov et al., 2012, 2014, 2016; Williams & Zank, 1994; Williams et al., 1995; Zank et al., 1996, 2012, 2017; Zhou & Matthaeus, 1990a, 1990b). We believe that the same description works here, but that a new source of neutral H other than the interstellar gas must be found and we believe that source is the Jovian system.

In this paper, we analyze Voyager magnetic field observations of low-frequency waves in the solar wind near Jupiter. The properties of the waves indicate the source is excitation by pickup H^+ and we establish a minimum ion production rate required to account for the waves. We demonstrate why these observations are unlikely to result from the ionization of interstellar neutral atoms. Using inferred turbulence rates and well-established per neutral ionization rates, a local neutral H density in the solar wind around Jupiter can be computed. While Kirsch et al. (1981) used the Voyager LECP instrument to infer the presence of neutral atoms upstream of Jupiter, there are no instruments on the Voyager spacecraft that can directly measure either the neutral H or the pickup H^+ at a few keV or less in the plasma frame, so we are left to infer the density of these populations based on the wave observations and known theory that has successfully explained wave observations due to newborn interstellar pickup ions. We also consider the possibility that proton acceleration by the Jovian bow shock could explain the observations and argue against this interpretation.

2. Data Overview

In this section we first provide an overview of our techniques and descriptions of the wave observations that are attributable to pickup H^+ in the near-Jupiter environment. We then attempt to explain the observations using known ion production rates for interstellar PUIs and show that this source cannot explain the observations shown here. Failing that, we restructure our analysis to uncover the likely ion production rates for an assumed Jovian source of neutrals.

Our discovery and analysis methods for the wave and control events are described in detail elsewhere (Argall et al., 2017, 2018; Hollick et al., 2018a). We use 1.96 s magnetic field data obtained from the National Space

Science Data Center (NSSDC). Data gaps are filled with badpoint flags, and the data are passed through an automated editor that removes data values that are several standard deviations away from the local mean value of the data and thereby considered unphysical. Daily spectrograms that include power and polarization parameters reveal wave intervals of anomalous bias in the polarization spectra and sometimes enhancement in the power over the range $f_{p,c} \leq f_{sc} \leq 4f_{p,c}$ where $f_{p,c}$ is the proton cyclotron frequency and f_{sc} is the fluctuation frequency as measured in the spacecraft frame. They also reveal times when wave signatures are not present and these intervals are used as controls in the analysis. We avoid interplanetary shocks that can be a source of energetic particles with moderately similar wave signatures (Bamert et al., 2004; Kennel et al., 1986; Lee, 1983; Smith, 1989), but the outbound crossings of the bow shock may be difficult to eliminate as possible explanations for the observations.

Once identified, we perform a similar analysis on the specific time interval taking care to avoid discontinuities and other features that might contaminate the computed spectra. Power spectra are obtained via Blackman-Tukey methods (Matthaeus & Goldstein, 1982) in both heliocentric coordinates and mean field coordinates (Belcher & Davis, 1971; Bieber et al., 1996). Power and polarization spectra are computed via FFT techniques (Fowler et al., 1967; Means, 1972; Mish et al., 1982; Rankin & Kurtz, 1970). The degree of polarization, D_{pol}, is the ratio of the polarized power to the total power in the fluctuations. It is computed using the diagonal terms of the power spectral matrix. The coherence, C_{oh}, derives from the off-diagonal terms in the power spectral matrix and offers a measure of the cross-component correlation of the fluctuations. The ellipticity, E_{lip}, is the ratio of the minimum to maximum axes of the fluctuation ellipse. We choose to associate the sign of the polarization with E_{lip} such that $E_{lip} > 0$ ($E_{lip} < 0$) denotes right-hand (left-hand) polarization in the spacecraft frame and $|E_{lip}| = 1$ ($E_{lip} = 0$) denotes circular (linear) polarization. The minimum variance direction is computed and taken to represent the direction of propagation relative to the mean magnetic field. This analysis is incapable of distinguishing between parallel propagation in the sunward and anti-sunward directions. Therefore, the angle between the minimum variance direction and the mean field, $\Theta_{kB} \equiv \arccos\left(\hat{\mathbf{k}} \cdot \hat{\mathbf{B}}\right)$ is represented such that $0° \leq \Theta_{kB} \leq 90°$.

Figure 1 shows an example of one such spectrogram of the magnetic field for Voyager 1 DOY 76 of 1979 when the spacecraft was 188 R_J from the planet. Top to bottom, the panels represent the radial component and magnitude of the ambient magnetic field, and the power, percent polarization, ellipticity, Θ_{kB}, and coherence of the magnetic fluctuations. The horizontal blue, red and pink lines mark the cyclotron frequencies of H^+, He^+, and O^+, respectively. The power is an ineffective way to find the waves we are searching for as the waves often show only a minor enhancement above the background spectrum. However, note the blue features in the ellipticity at $f_{sc} > f_{p,c}$ before and after noon. This represents times and frequencies where the fluctuations are left-hand polarized in the spacecraft frame. These same intervals and frequencies show coherence and percent polarization as well as field-aligned minimum variance directions $\Theta_{kB} \simeq 0°$. We will revisit one of these examples below. We find our wave examples by examination of these daily spectrograms.

Figure 2 shows the trajectory of the two spacecraft through the Jovian system where the spacecraft enter at the top of each panel and exit toward the bottom. The coordinates are jovigraphic (Bagenal et al., 2017) and the trajectory data was obtained from the SEDR files provided by the NASA Planetary Data System. Black hatch marks represent recognized shock crossings, red dashed lines represent the beginning and end of the interval excluded from Hollick et al. (2018a, 2018b, 2018c), and the red triangles represent the wave times. The black dashed curves represent nominal bow shock locations. However, the shock is well-known to move significantly with changing solar wind conditions (Lepping et al., 1981). Note that while both spacecraft follow similar trajectories inbound, Voyager 2 passes significantly further down the Jovian magnetotail and exits the magnetosphere further from the planet. Both spacecraft remain largely within the (X, Y) plane with only minimal excursion in the Z direction which is approximately the direction orthogonal to the orbital plane of the Jupiter. The Jovian bow shock is significantly flattened in the Z direction, or extended in the Y direction, and it has been argued that this results in the propagation of large-scale disturbances across the shock surface (Lepping et al., 1981). The wave events observed on the inbound pass that are not attributable to newborn interstellar PUIs have been described as either shock associated or arising from leaked heavy ions (Goldstein et al., 1983, 1984, 1985; Smith & Lee, 1986; Smith et al., 1983, 1984). We are primarily interested in the waves observed on the outbound pass of either spacecraft and we find that there are some events of interest to this analysis beyond the outbound border of the previously excluded data.

Figure 3 shows a different representation of the trajectories of the Voyager 1 and 2 spacecraft as they transit the Jovian environment along with the times and durations of the wave events. Units are in Jovian radii and the

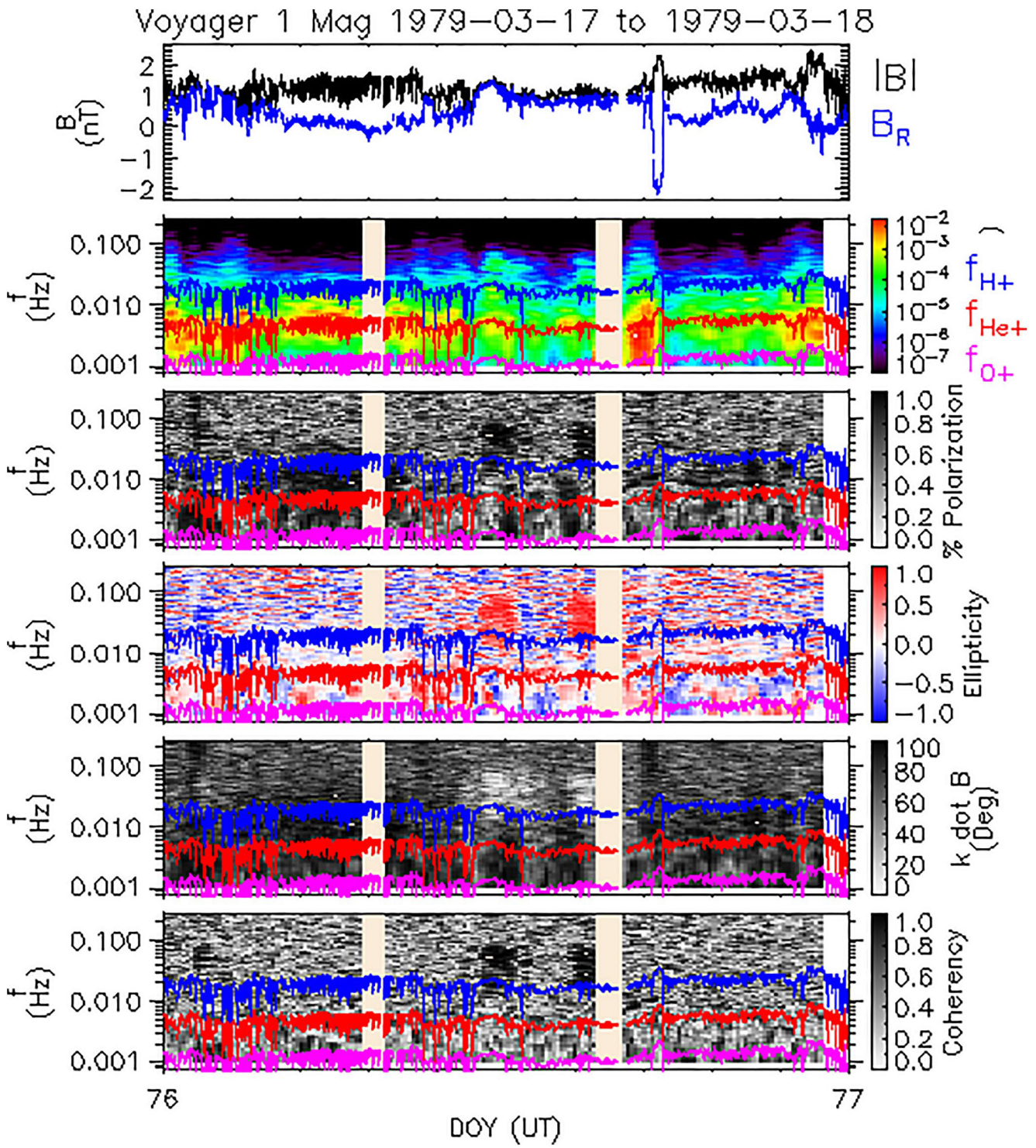

Figure 1. Example daily magnetic spectrogram for Voyager 1 DOY 076 of 1979. (top to bottom) Timeseries for **|B|** (black) and radial component B_R (Blue); total power spectrum (trace of the power spectral density matrix); percent polarization (degree of polarization); ellipticity; angle between the minimum variance direction and mean magnetic field Θ_{kB}; and coherence. Horizontal lines are the H^+ cyclotron frequency $f_{p,c}$ (blue), He^+ cyclotron frequency $f_{He,c}$ (red), and O^+ cyclotron frequency $f_{O,c}$ (pink). Note two blue patches near midday that are indicative of left-hand polarized fluctuations at $f_{sc} \geq f_{p,c}$.

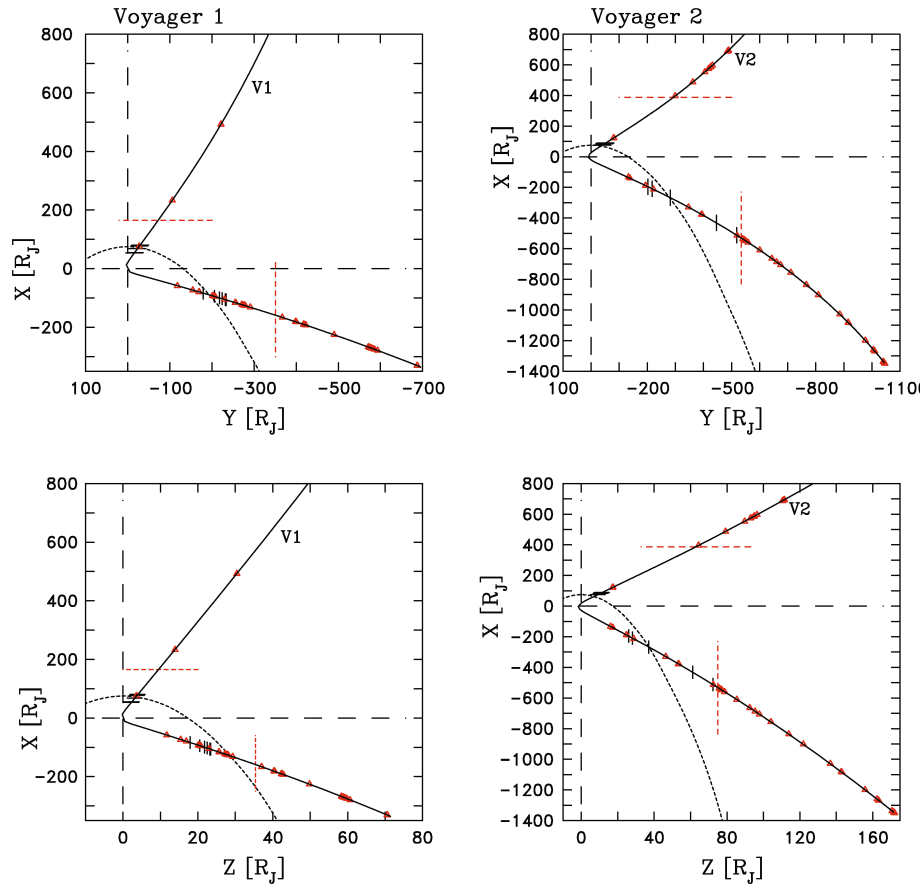

Figure 2. Trajectory of the Voyager 1 and 2 spacecraft through the Jovian system. Black hash marks along the trajectory represent recognized shock crossings, red triangles represent the wave events, the red dashed lines mark the beginning and end of data intervals that were omitted from the earlier interstellar source analysis, and the black dashed curves represent nominal shock locations.

same jovigraphic coordinates as were used in Figure 2. The vertical solid red line marks the closest approach to the planet. The region between the vertical dashed red lines again mark the region for wave and control events that were excluded from the previous study of solar wind observations resulting from interstellar PUIs. The vertical dashed black lines mark the shock crossings as best they are known (Bridge et al., 1979a, 1979b; Richardson, 2002). It is likely that Voyager 2 experienced additional, poorly resolved shock crossings on the outbound path (Kurth et al., 1981). Tables 1 and 2 list the times of closest approach, the established times within the magnetosphere, and the range of times that were excluded from the earlier study of interstellar PUIs. The bottom of the figure shows the time and duration of wave events (triangles) studied here. Red (green) triangles represent events when Voyager Plasma Science (PLS) (Bridge et al., 1977) data is available (unavailable). Tables 3 and 4 list the times and durations of the wave events studied here. Black circles represent the times when control intervals lacking wave signatures attributable to PUIs were used.

Bridge et al. (1979a, 1979b) and Ness et al. (1979a, 1979b) show the trajectory of both spacecraft through the Jovian magnetosphere. Voyager 1 crossed the bow shock inbound several times from DOYs 59 through 61 and outbound over DOYs 77 through 81. Our exclusion of wave events from the earlier interstellar PUI analysis and our incorporation of wave events here spans a larger interval than just the Jovian magnetosphere. None of the wave or control events observed by Voyager 1 that are studied here are seen within the Jovian magnetosphere during the inbound pass. Several of the wave events described here are seen during the outbound pass and close to the outbound shock crossings. This raises the possibility of shock accelerated ions being the source of the waves that we will address in Section 4.3. Except for one wave event (11:00–13:00 UT on DOY 76), the wind speeds, densities, and field strengths are typical of solar wind conditions. During this one event, the wind speed is 285 km s^{-1}, the density is 0.14 cm^{-3}, the field strength is 1.2 nT, and the Mach number is 4.1. Nothing about

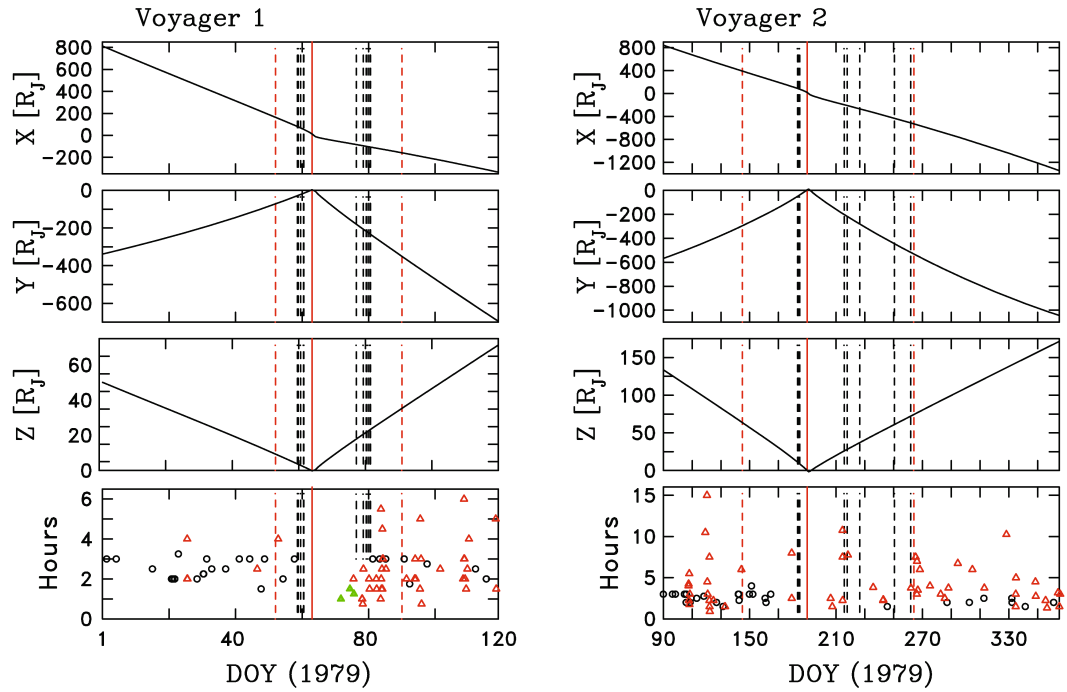

Figure 3. (top to bottom) Trajectory of the Voyager spacecraft through the Jovian system. Trajectory is in S3 coordinates. Time and duration of the wave and control intervals used in this study. Red (green) triangles represent wave intervals when PLS data are (are not) available. Black circles represent control intervals. Only control intervals when PLS data are available are used here. Red vertical solid lines represents the times of closest approach to Jupiter. Black vertical dashed lines mark the known shock crossings. Red vertical dashed lines mark the boundaries of time intervals that were excluded from the previous interstellar pickup ion studies.

the parameters describing this one event negates the theoretical expressions used here with the possible exception of PUI production from interstellar neutral atoms which fails to consider the presence of the Jovian bow shock. While these could be solar wind conditions, they are atypical of the other intervals. Both Bridge et al. (1979a) and Ness et al. (1979a) report the spacecraft to be within the Jovian magnetosheath at this time.

The Voyager 2 inbound crossings occurred on DOYs 183 through 186. The Voyager 2 spacecraft headed deeper down the tail and remained within the magnetosphere longer than Voyager 1 with three outbound shock crossings reported on DOY 215 (Bridge et al., 1979b; Ness et al., 1979b). This places five of the more significant wave observations that we report on DOYs 206, 207 and 214 behind the Jovian bow shock and inside the Jovian magnetosheath. Bridge et al. (1979b) state "…there may be additional crossings after day 215." The wave observations that most interest us extend to DOY 242 at least and there is no clear analysis available that determines the times of shock crossings at these later dates.

The remainder of the Voyager 2 wave observations cannot reliably be placed in the solar wind, but related analyses do place the spacecraft in the general proximity of the bow shock throughout the time interval analyzed here. These observations also do not rule out the likelihood that the spacecraft is within the solar wind at the time of the wave observations. None of the wave events studied here have been reported previously as attributable to shock acceleration or magetospheric leakage of protons or heavy ions (Goldstein et al., 1983, 1984, 1985; Smith & Lee, 1986; Smith et al., 1983, 1984). The analysis by Kurth et al. (1981) of nonthermal continuum

Table 1
Times of Jupiter Encounters for the Voyager Spacecraft

S/C	CA date	CA year/DOY	Magnetosphere year/DOY	Shocks year/DOY	Study interval year/DOY
V1	5 March 1979	1979/064	1979/060-074	1979/059-081	1979/053-091
V2	9 July 1979	1979/190	1979/185-215	1979/183-215	1979/145-264

Table 2
Jupiter Shock Crossing Times

S/C	Shock time [DOY::Hr:Mn] UT	Shock distance [R_J]	Reference
V1	059::14:34	85.7	Bridge et al. (1979a)
V1	059::19:52	82.2	Bridge et al. (1979a)
V1	060::12:26	71.7	Bridge et al. (1979a)
V1	061::09:50	57.8	Bridge et al. (1979a)
V1	061::13:08	55.7	Bridge et al. (1979a)
V1	077::07:04	199.2	Bridge et al. (1979a)
V1	079::08:27	227.0	Bridge et al. (1979a)
V1	080::07:11[a]	240.0	Bridge et al. (1979a)
V1	080::19:36[b]	241.0	Bridge et al. (1979a)
V1	081::09:43	246.0	Bridge et al. (1979a)
V1	081::13:02	248.0	Bridge et al. (1979a)
V2	183::06:19	98.8	Bridge et al. (1979b)
V2	183::16:22	98.8	Bridge et al. (1979b)
V2	183::16:43	98.6	Bridge et al. (1979b)
V2	183::16:50	98.5	Bridge et al. (1979b)
V2	183::16:51	98.5	Bridge et al. (1979b)
V2	183::19:24	97.3	Bridge et al. (1979b)
V2	184::17:36	86.6	Bridge et al. (1979b)
V2	215::14:41	282.2	Bridge et al. (1979b)
V2	215::16:25	283.0	Bridge et al. (1979b)
V2	215::17:03	283.3	Bridge et al. (1979b)
V2	217::17:00[c]	226.2	Kurth et al. (1981)
V2	226::12:30[d]	226.4	Kurth et al. (1981)
V2	250::12:30[e]	225.9	Kurth et al. (1981)
V2	261::21:53[f]	225.4	Kurth et al. (1981)

Note. Superscripts a–f represent approximate times.
[a]Between 080::06:07–080::08:16 UT. [b]Between 080::08:16–081::06:57 UT. [c]Between 215::17:30–219::16:30 UT. [d]Between 222::05:00–230::20:00 UT. [e]Between 242::00:00–259::01:00 UT. [f]Between 260::05:00–263::14:45 UT.

radiation "…has led to the identification of brief encounters with the Jovian magnetosphere…" during the outbound trajectory of both spacecraft. Their analysis does not determine the times of shock crossings and does not reliably determine the location of the spacecraft either in the magnetosphere, magnetosheath, or solar wind during the times when the waves reported here are observed. Keeping these limitations in mind, we can interpret the results of Kurth et al. (1981) as follows: They state that the first outbound shock crossing by Voyager 1 occurs somewhere between days 74 and 116, which is consistent with the report by Bridge et al. (1979a). They offer no indication of additional outbound shock crossings by the Voyager 1 spacecraft. There are apparent additional outbound shock crossings by Voyager 2 beyond the DOY 215 crossing reported by Bridge et al. (1979b). The first shock crossing reported by Kurth et al. (1981) is between DOYs 222 and 230. The outbound shock crossings reported on DOY 215 by the PLS instrument are not reported in this analysis. There are additional solar wind observations through DOY 241 with an implied shock crossing sometime between DOYs 242 and 259. Voyager 2 is again behind the shock some time on DOY 259 and early 260 and is again in the solar wind on by 14:45 UT on DOY 263. Kurth et al. (1981) finds no further evidence of shock involvement through the end of the year.

Wherever the more distant shock crossings occur, we can assume that the shock is weak at that point because of its distance down the flanks. We have been unable to find the implied more distant shock crossings in the data and the fact that they are not reported by the instrument teams lends further credence to this assertion. Therefore, to whatever degree the boundary still exists as a shock, we can reasonably assume that the shock is weak.

Figure 4 shows the ambient plasma conditions for the wave and control intervals shown in Figure 3. All are within the acceptable range for solar wind measurements (Parker, 1963). The average winding angle for control intervals is $\Theta_{BR} > 60°$ as expected, but wave intervals show a large number of events with $\Theta_{BR} < 60°$ which tend to occur in rarefaction regions (Gosling & Skoug, 2002; Murphy et al., 2002; Schwadron, 2002; Schwadron & McComas, 2005). Pickup ions tend to produce relatively weak instabilities that require the lower background spectra often seen in rarefaction regions in order to be observable (Aggarwal et al., 2016; Argall et al., 2017; Cannon, Smith, Isenberg, Vasquez, Joyce, et al., 2014; Fisher et al., 2016; Hollick et al., 2018b; Marchuk et al., 2021). With only a few exceptions, the wind speed falls in the nominal range $300 < V_{SW} < 500$ km s^{-1}. The proton density N_P also falls in the nominal range $0.1 \leq N_P \leq 1$ cm^{-3}, but wave intervals do tend to show lower solar wind proton densities than the control intervals. Some of the wave intervals with higher than nominal B also have lower than average N_P. This is also consistent with the location of these waves within the type of rarefaction region where the ambient magnetic field threads through the rarefaction. Proton temperatures, T_P, are typical for the solar wind at this distance as is the proton beta, β_P. Alfvén speeds, V_A are typical, although the few wave events with higher than expected B and lower than expected N_P have a correspondingly higher than expected V_A. Still, nothing is outside the acceptable range for solar wind measurements. With only a few exceptions, the Alfvén Mach number $M_A < 20$. Despite the fact that these measurements are all consistent with solar wind conditions, there is evidence as described above that indicates that a few of the Voyager 2 wave events occur within the magnetosheath of the planet. Given that the spacecraft is far downstream where the bow shock is likely to be weak, it is not unexpected that the sheath conditions would be in general agreement with nominal solar wind conditions. We do not believe that this uncertainty affects the analysis described here.

Table 3
Voyager 1 Wave Analyses

Times [DOY::Hr:Mn]	$f_{p,c}$ [mHz]	E_{lip}	$(dH^+/dt)^{LISM}$ [10^{-10} cm^{-3} s^{-1}]	$(dH^+/dt)^{MIN1}$ [10^{-10} cm^{-3} s^{-1}]	$(dH^+/dt)^{MIN2}$ [10^{-10} cm^{-3} s^{-1}]
26::11:00–26::15:00	0.81	−0.82	1.31	1.18	0.37
26::11:00–26::13:00	0.81	−0.80	1.33	1.02	0.44
26::13:00–26::15:00	0.82	−0.83	1.30	1.44	0.66
53::19:30–53::23:30	10.3	−0.81	2.10	54.2	5.38
72::16:00–72::17:00	48.8	+0.91	5.67	7.21	44.3
75::09:00–75::10:30	17.8	−0.73	5.70	40.2	6.28
76::11:00–76::13:00	1.77	−0.66	2.46	128	25.2
76::14:00–76::15:15	1.70	−0.79	5.72	30.8	108.3
79::10:30–79::13:00	1.22	−0.53	3.42	965	28.6
79::00:30–79::01:30	1.49	−0.62	3.34	1,662	376.8
79::02:00–79::03:00	1.49	−0.62	3.07	1,694	380.6
79::05:30–79::06:15	1.19	−0.50	3.47	5,830	400.0
81::07:00–81::08:30	8.87	−0.67	2.65	918	1272.
81::03:00–81::05:00	8.24	−0.44	2.34	779	289.3
83::07:30–83::09:30	5.98	−0.67	2.42	175	159.8
83::10:00–83::11:30	5.84	−0.67	1.91	197	67.8
84::17:00–84::22:30	10.6	−0.79	2.82	69.9	46.4
84::15:00–84::16:00	9.17	−0.58	3.26	106	37.2
84::19:00–84::21:00	9.76	−0.85	2.68	83.4	14.4
84::21:00–84::22:30	12.2	−0.83	3.14	40.0	59.2
85::00:00–85::02:30	11.2	−0.76	2.98	9.94	49.7
85::03:00–85::04:30	9.91	−0.62	2.21	196	3.83
85::04:30–85::07:30	11.3	−0.76	2.83	151	98.0
85::08:30–85::11:30	9.71	−0.47	2.80	108	103.5
85::03:00–85::07:30	10.7	−0.75	2.74	173	26.3
86::05:00–86::07:30	10.1	+0.70	1.90	24.7	113.8
91::18:00–91::19:30	18.5	−0.22	2.34	48.8	7.01
92::09:00–92::11:00	13.3	+0.58	2.01	48.8	26.1
94::20:00–94::22:00	20.7	−0.31	2.59	16.3	12.6
95::00:00–95::03:00	20.7	—	2.29	14.6	13.0
95::03:30–95::05:30	20.7	—	1.81	11.8	11.5
96::11:00–96::12:30	18.2	−0.72	2.06	3.11	2.04
96::12:30–96::17:30	16.1	−0.76	2.49	4.86	5.02
96::18:00–96::21:00	15.8	−0.77	2.05	3.93	4.72
96::21:45–96::22:30	15.7	−0.77	1.79	3.16	2.39

Figure 5 shows examples of the analysis used here. Figure 5 (left) shows a textbook example of low-frequency waves excited by pickup H^+. The red lines represent our fit to the background spectra. There is an enhancement in fluctuation power at $f_{sc} > f_{p,c}$ that coincides with an increase in both D_{pol} and C_{oh} while $E_{lip} \simeq -1$ and $\Theta_{kB} \simeq 0°$ at the same frequencies. The apparent double-peaked nature of the wave enhancement may or may not be statistically significant in so far as it suggests an interruption of the normal scattering process. Figure 5 (middle) shows how a textbook spectrum can become complicated by unresolved physics. The same signatures of a pickup H^+ source are evident, but the wave signatures extend to significantly lower frequencies $f_{sc} \simeq 3$ mHz. Either there are

Table 4
Voyager 2 Wave Analyses

Times [DOY::Hr:Mn]	$f_{p,c}$ [mHz]	E_{lip}	$(dH^+/dt)^{LISM}$ [10^{-10} cm^{-3} s^{-1}]	$(dH^+/dt)^{MIN1}$ [10^{-10} cm^{-3} s^{-1}]	$(dH^+/dt)^{MIN2}$ [10^{-10} cm^{-3} s^{-1}]
107::13:45–107::18:00	8.83	−0.61	4.65	9.01	2.69
107::18:00–107::20:15	8.38	−0.68	4.51	7.52	3.89
107::12:00–107::16:00	8.81	−0.55	4.83	9.42	3.40
108::00:30–108::06:00	10.6	−0.66	3.72	8.31	2.06
108::10:30–108::13:30	10.2	−0.45	3.48	7.39	1.55
108::04:15–108::06:00	10.7	−0.50	4.06	5.24	1.01
119::04:30–119::15:00	12.5	−0.47	2.07	3.53	2.70
120::07:30–120::22:30	11.7	−0.66	2.06	1.48	0.91
120::19:30–120::22:30	12.3	−0.56	2.12	2.28	1.09
120::13:30–120::18:00	12.3	−0.65	2.15	1.15	0.78
122::00:45–122::08:15	11.6	−0.61	1.99	3.10	1.73
122::00:45–122::03:00	11.8	−0.46	1.91	4.39	3.27
122::03:00–122::04:30	11.0	−0.39	2.02	5.18	3.22
122::07:20–122::08:15	12.0	−0.80	2.02	1.51	1.78
124::18:45–124::21:00	10.3	−0.51	2.21	3.01	1.55
132::21:00–132::22:30	4.60	−0.49	1.54	3.24	1.27
144::06:00–144::12:00	2.30	−0.41	1.48	2.61	0.99
179::04:00–179::12:00	9.95	+0.09	1.82	4.21	0.48
179::05:00–179::07:30	10.0	+0.29	1.82	3.57	0.59
206::06:00–206::08:30	35.7	+0.08	5.70	1553.	310.2
207::09:00–207::10:30	32.1	−0.68	6.98	164.3	74.5
214::11:15–214::22:00	5.75	−0.34	2.40	255.6	123.3
214::13:30–214::15:45	6.99	−0.63	2.40	321.6	146.8
214::11:15–214::18:45	6.52	−0.37	2.40	377.5	219.9
218::05:45–218::13:30	41.4	−0.40	13.7	275.9	199.0
235::18:45–235::22:35	8.61	−0.71	2.15	333.3	127.7
242::15:00–242::17:15	11.2	−0.49	6.07	51.9	56.3
242::20:00–242::22:20	10.6	−0.16	6.86	76.8	55.8
262::00:45–262::04:30	31.7	−0.75	10.4	196.5	83.1
265::07:30–265::15:00	34.4	−0.57	3.60	1.82	1.76
266::03:00–266::06:00	27.3	−0.80	2.17	0.66	0.68
266::06:00–266::13:00	21.6	−0.67	2.02	2.45	2.52
266::19:00–266::22:30	15.1	+0.06	1.77	7.32	6.06
268::06:00–268::12:00	19.2	−0.21	1.81	4.20	1.89
275::06:00–275::10:00	7.10	−0.24	2.25	4.39	1.46
282::15:45–282::18:45	6.59	+0.35	2.90	11.0	7.78
285::12:00–285::14:30	21.0	−0.33	7.29	25.1	19.9
288::02:15–288::06:00	7.75	+0.58	2.35	14.4	11.1
294::13:45–294::20:30	6.34	−0.34	4.24	15.3	6.90
304::16:30–304::22:30	8.69	−0.59	2.68	3.37	1.50
313::00:00–313::03:45	13.1	−0.60	5.50	21.7	13.9
328::08:15–328::18:30	7.19	−0.83	2.45	1.09	0.47

Table 4
Continued

Times [DOY::Hr:Mn]	$f_{p,c}$ [mHz]	E_{lip}	$(dH^+/dt)^{LISM}$ [10^{-10} cm^{-3} s^{-1}]	$(dH^+/dt)^{MIN1}$ [10^{-10} cm^{-3} s^{-1}]	$(dH^+/dt)^{MIN2}$ [10^{-10} cm^{-3} s^{-1}]
334::19:30–334::22:30	20.7	−0.63	4.37	0.97	0.89
334::19:30–334::21:00	20.1	−0.75	4.76	1.13	0.61
335::00:15–335::05:15	20.1	+0.70	3.19	3.80	1.67
348::12:00–348::16:30	15.9	−0.35	3.81	5.71	1.44
355::13:30–355::15:45	8.66	−0.50	5.78	2.36	1.67
356::13:40–356::15:00	8.56	−0.79	7.03	3.48	1.08
364::02:50–364::06:00	11.2	−0.63	5.33	3.64	0.96
365::03:00–365::04:30	8.35	−0.62	4.47	4.94	1.16
365::16:30–365::19:30	6.63	+0.26	3.03	44.6	12.8

significantly more energetic particles present or there are heavier PUIs such as He^+ present. Approximately 30% of the wave events studied here show wave signatures at $f_{sc} < f_{p,c}$. Figure 5 (right) shows a similar spectrum to the middle panel with the wave signature extending to frequencies $f_{sc} < f_{p,c}$, but with a steeper than normal f^{-2} power spectrum over the frequency range $0.005 < f_{sc} < 0.1$ Hz.

Our analysis of the polarization and power levels of the wave and control intervals is summarized in Figure 6. Curves in the top panels represent the trace of the power spectral density matrix "Tr" and the power spectrum of the fluctuations aligned with the mean magnetic field labeled "Z." One thing that becomes immediately evident is that the polarization parameters of the waves is readily distinguishable from the control intervals while the power levels are less distinctive. To compute the average polarization parameters D_{pol}, C_{oh}, E_{lip} and Θ_{kB}, we average the spectra over the range $f_{p,c} \le f_{sc} \le 2f_{p,c}$. The frequency-averaged values of D_{pol} and C_{oh} show generally elevated values relative to the control intervals. This is what we see in waves excited by newborn interstellar PUIs (Aggarwal et al., 2016; Fisher et al., 2016; Cannon, Smith, Isenberg, Vasquez, Murphy, & Nuno, 2014; Hollick et al., 2018a). The average E_{lip} parameters show the waves are generally left-hand polarized in the spacecraft frame with a few exceptions. Again, exceptions like this exist for the interstellar PUI source as well and are not fully understood, but they do not rule out the source interpretation given here. Minimum variance directions are generally field-aligned $\Theta_{kB} \le 30°$ as predicted by theory. This is all consistent with what has been seen before for waves due to newborn interstellar PUIs.

Power spectra are fit as demonstrated in Figure 5 to obtain the background power level $P_B(f_{p,c})$ at $f_{p,c}$ by omitting the frequencies that exhibit enhanced power in the likely range of waves due to pickup H^+. Here we see something unexpected: there are wave intervals within the exclusion zone from the earlier interstellar waves analysis where the background spectrum is unusually high when compared to the background power levels outside the exclusion zone that are more typical of events arising from newborn interstellar PUIs. Since newborn interstellar PUIs are of very low density and the instability associated with them is correspondingly weak, the associated waves seen at this heliocentric distance require tens of hours or more to grow to observable levels and the growth rate must exceed the rate at which turbulence absorbs the wave energy or the waves are rendered unobservable (Hollick et al., 2018b). The elevated background spectrum increases the time or PUI density required to reach observable power levels for the waves as well as the turbulence level that the instability must overcome. This is the first indication that some of these wave events cannot be explained by newborn interstellar pickup H^+. Lastly, Figure 6 shows the ratio of measured wave power to background power P_W/P_B at the spacecraft-frame frequency where the enhancement above background is greatest over the range $f_{p,c} \le f_{sc} \le 4f_{p,c}$. Many of the wave intervals show significant enhancement above the background level. As expected, control intervals do not.

3. Theory

A theoretical description of waves due to a PUI source requires the following: the recognition of a neutral atom source and an ionization process of sufficient strength to produce the density of PUIs required for instability and wave growth, an understanding of the instabilities that results in wave excitation, an understanding of the phase

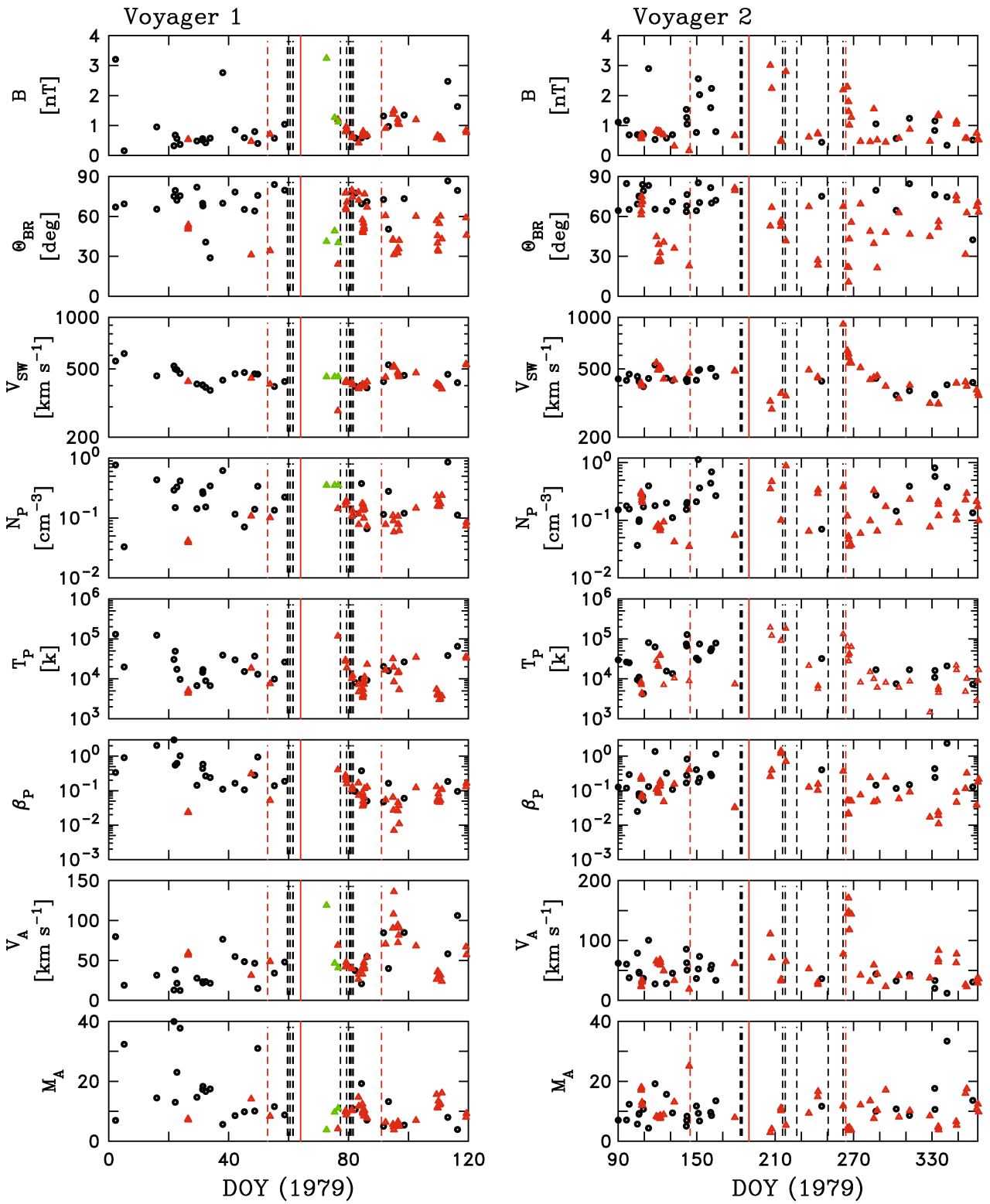

Figure 4. Ambient plasma parameters for wave events (red and green triangles) and control intervals (black circles). (top to bottom) Magnetic field intensity B, angle between the mean field and the radial direction Θ_{BR}, average solar wind speed V_{SW}, thermal proton density N_P, thermal proton temperature T_P, plasma beta β_P, Alfvén speed V_A, and Mach number M_A. Nominal plasma values are used when PLS data is not available (green symbols). Solid and dashed red and black lines have the same interpretation as before.

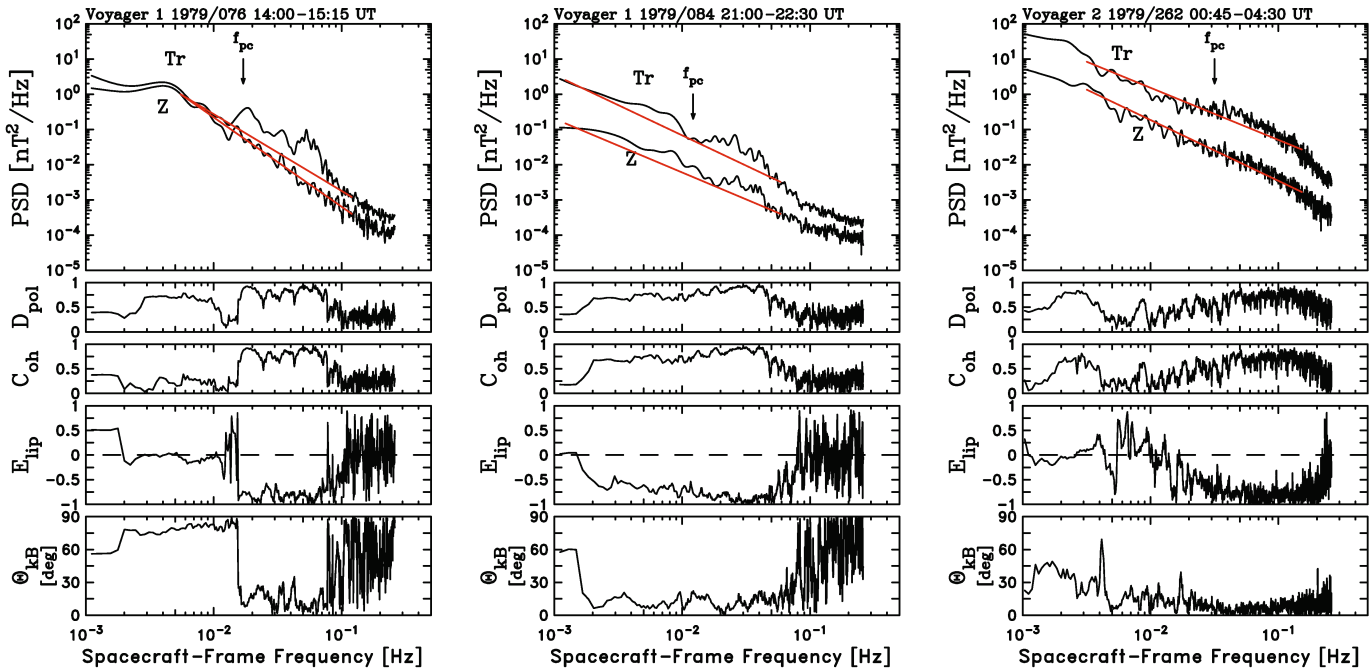

Figure 5. Examples of wave analyses used here. Top to bottom, the trace of the power spectral density matrix "Tr" and component aligned with the mean magnetic field "Z," degree of polarization, coherence, ellipticity, and angle between the minimum variance direction and the mean magnetic field. (left) A textbook example of a wave spectrum excited by pickup H^+. (middle) A more complicated example of waves excited by H^+ that extends to lower frequencies. This may be the result of particle energization above the pickup energy or the presence of heavier pickup ions. (right) A spectrum with waves due to pickup H^+ and likely exhibiting a dissipation spectrum at higher frequencies due to the ambient turbulence.

space distribution of newborn PUIs and how it relates to the instabilities, and an adequate wave growth to overcome the turbulent processes responsible for the transport and dissipation of energy. The problem associated with explaining the observations described here as arising from an interstellar source is that the interstellar neutral H atoms and the associated ionization processes are well-known and insufficient to produce wave growth in excess of the turbulence rates. This implies that the turbulence does not allow for the long-term accumulation of wave energy over the time scales required for growth due to the interstellar source (Hollick et al., 2018b).

Whatever the source of the neutral atoms, if the pickup process produces ions with negligible initial velocity in the Sun's frame of reference, we can apply the theory of wave excitation by interstellar PUIs (Lee & Ip, 1987) under the two assumptions that the local mean magnetic field is radial and the plasma remains in a region of constant PUI production over the time that the wave grows to an observable level. The radial field assumption can be relaxed so long as the ion's motion along the field is sufficient for the resonance to be dominated by neglecting the wave frequency. The time-asymptotic wave intensities of $I_{\pm}(k, t)$ are given by:

$$I_{\pm}(k,\infty) = \frac{1}{2}\left[C(k)^2 + 4I_{+}(k,0)I_{-}(k,0)\right]^{1/2} \pm \frac{1}{2}C(k), \tag{1}$$

where $I_{+}(k, 0)$ ($I_{-}(k, 0)$) is the background spectrum at wavenumber k for anti-sunward (sunward) propagating fluctuations which we take to exist at $t = 0$. The theory is one-dimensional in that only waves propagating parallel to the magnetic field are considered. For the I_{-} sunward propagating waves, negative k representing right-hand polarized fast-mode waves and positive k representing left-hand polarized Alfvén waves. For the I_{+} anti-sunward propagating waves, the association is reversed. The total spectrum is obtained by summing over the four permutations of Equation 1 (i.e., $I_{tot}(k, \infty) = I_{+}(+k, \infty) + I_{+}(-k, \infty) + I_{-}(+k, \infty) + I_{-}(-k, \infty)$).

The wave enhancement term is given by

$$C(k) = I_{+}(k,0) - I_{-}(k,0) + 2\pi m_i n_i V_A |\Omega_{i,c}| k^{-2} \left[\Omega_{i,c} k^{-1} v_0^{-1} - \frac{\left(\Omega_{i,c} k^{-1} v_0^{-1} - \mu_0\right)}{|\Omega_{i,c} k^{-1} v_0^{-1} - \mu_0|}\right], \tag{2}$$

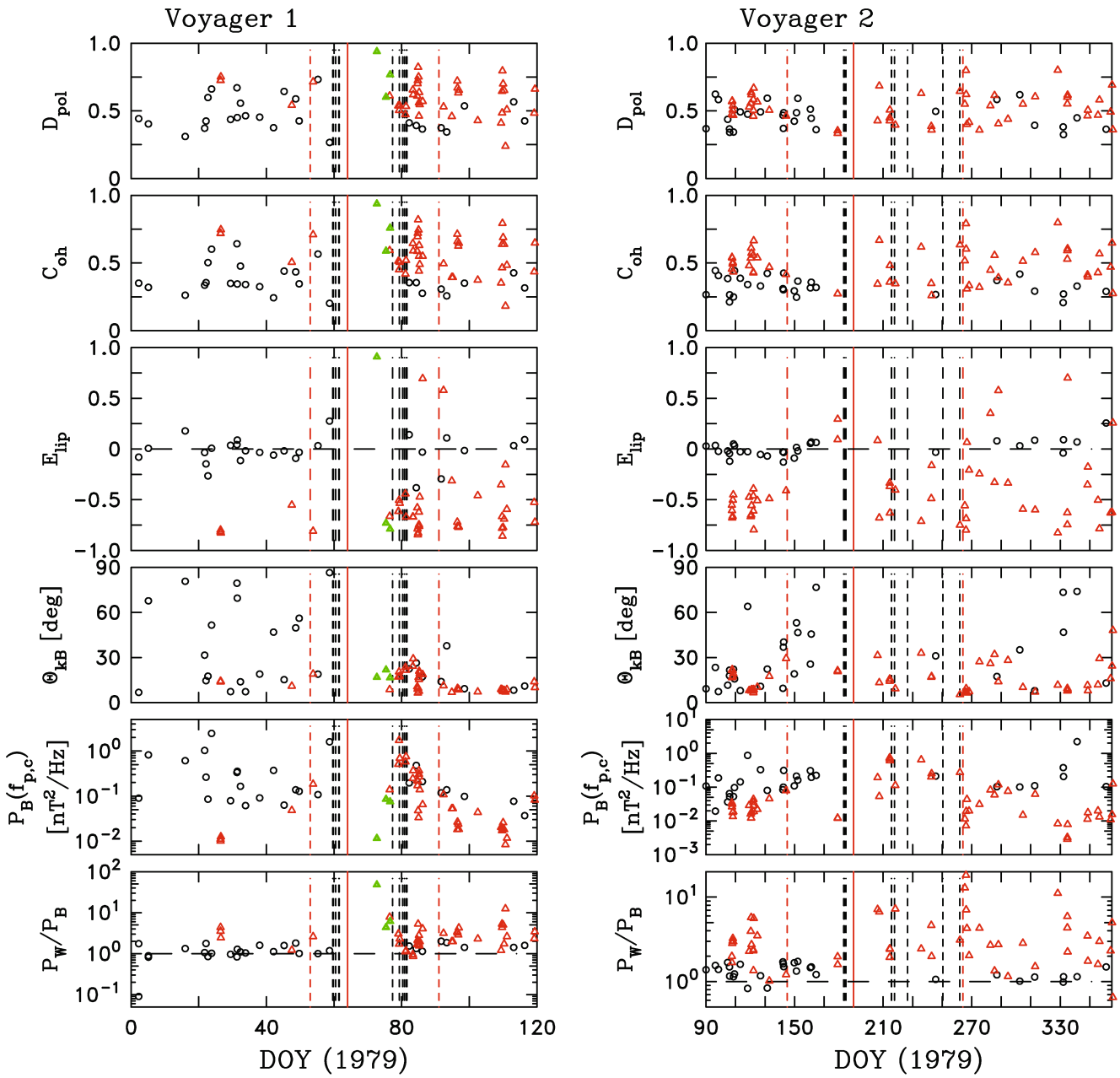

Figure 6. Polarization analysis of wave and control intervals averaging over the range $f_{p,c} \leq f_{sc} \leq 2f_{p,c}$ using the same symbols as Figure 4. (top to bottom) Degree of polarization D_{pol}, coherence C_{oh}, ellipticity E_{lip}, and angle between the minimum variance direction and the mean magnetic field Θ_{kB}, background spectral power at the proton cyclotron frequency, and the ratio of the measured power to the background power at the peak of the spectrum in the frequency range given.

where m_i is the pickup ion mass, n_i is the pickup ion number density, $\Omega_{i,c} = 2\pi f_{i,c}$ with $f_{i,c} = e_i B/(2\pi m_i c)$ being the ion cyclotron frequency, e_i is the charge of the pickup ion, B is the local magnetic field intensity, c is the speed of light, V_A is the Alfvén speed, v_0 is the PUI speed in the plasma frame (taken to be equal to the solar wind speed, V_{SW}) and μ_0 is the pitch angle of the newborn pickup ions. The background terms are taken to be $I_+(k,0) = I_-(k,0) = (1/4) I_{tot}(k_{i,c},0)(k/k_{i,c})^{-5/3}$, where $I_{tot}(k_{i,c}, 0)$ is the total background intensity ($=I_+(+k_{i,c}, 0) + I_-(+k_{i,c}, 0) + I_+(-k_{i,c}, 0) + I_-(-k_{i,c}, 0)$) at the ion cyclotron frequency where $|k_{i,c}|$ is given by $2\pi f_{i,c}/V_{SW}$.

Newly ionized PUIs are expected to scatter to near-isotropy in a small number of cyclotron periods, which is very short compared to the time for wave growth. Thus, we can assume that the wave spectrum evolves through a series of quasi-stationary asymptotic values that are predicted by the above formalism. We can then obtain a rate of

wave growth by taking the derivative relative to the rate of ion production (Aggarwal et al., 2016; Cannon, Smith, Isenberg, Vasquez, Joyce, et al., 2014; Fisher et al., 2016; Hollick et al., 2018b; Joyce et al., 2010):

$$\frac{dE_W}{dt} = R_{ac} \times 10^{10} \times 10^{-5} \left(\frac{2\pi f_w}{V_{SW}}\right) \left(\frac{21.8^2}{N_P}\right) \frac{1}{3600}, \tag{3}$$

where the factor 21.8 converts the magnetic field to Alfvén units, 10^{10} converts Gauss^2 to nT^2 and 10^{-5} converts cm to km, f_w is the spacecraft-frame frequency where the wave power is seen to peak (Hollick et al., 2018a), V_{SW} is given in km s^{-1}, and N_P is given in cm^{-3}. R_{ac} is given by $[I_{peak}(t_{acc2}) - I_{peak}(t_{acc1})]/[t_{acc2} - t_{acc1}]$, where t_{acc2} and t_{acc1} are two different accumulation times and $I_{peak}(t_{acc})$ is $I_{tot}(k, \infty)$ evaluated at the peak of the wave enhancement using n_i equal to t_{acc} times the newborn PUI production rate. For this calculation, t_{acc1} is the minimum accumulation time that produces a wave enhancement in the computed wave spectrum (i.e., a local maximum) and $t_{acc2} = t_{acc1} + 20$ hr. We have experimented with other values of t_{acc2} without finding significant sensitivity to the value chosen.

There are time scales for the turbulent transport of energy through the spectrum and characteristic lifetimes for the individual fluctuations. These vary depending on the specific theory for the turbulent dynamics. We will adopt the most traditional view that has come to be recognized as a likely explanation for the dominant two-dimensional (2D) fluctuations with wave vectors that are quasi-perpendicular to the mean magnetic field (Bieber et al., 1996; Dasso et al., 2005; Hamilton et al., 2008; Leamon et al., 1998; Matthaeus et al., 1990; Smith et al., 2013). This is a rescaling of Kolmogorov (1941) suitable for MHD (Leamon et al., 1999; Matthaeus & Velli, 2011; Matthaeus & Zhou, 1989; Smith, 2009). Rescaling the overall amplitude of the cascade rate per unit mass ϵ to match the observed proton heating rate at $R \leq 1$ AU (Montagud-Camps et al., 2018; Vasquez et al., 2007), we obtain a general expression that we can apply to the observations here at 5 AU:

$$\epsilon = \frac{f^{5/2}[E(f)]^{3/2} \cdot 21.8^3}{V_{SW} N_P^{3/2}} \tag{4}$$

where $E(f)$ is the measured magnetic field power spectral density in units of nT^2 Hz^{-1}, which is assumed to vary as $f^{-5/3}$. N_P and 21.8^3 are part of the conversion of the magnetic field to Alfvén units. We assume equipartition of kinetic and magnetic energy. By this expression, ϵ is given in units of km^2 s^{-3}.

Having now characterized the waves, control intervals, and the ambient plasma conditions when they are observed, we move to analyze the observations in terms of possible sources.

4. Data Analysis

The above formalism is applied in two different ways. We first compute the production rate of H^+ ions from a known density of interstellar neutral atoms and use this as input for calculating the wave growth rates for the observations shown here. The resulting production of H^+ is insufficient to explain the existence of the waves within the previous exclusion intervals. We then set the wave growth rates equal to the turbulence rates to compute the lower limits for the production of H^+ that are required for wave observability. This method produces a lower limit for ionization because in practice the wave growth rate will exceed the turbulence rate and produce an enhancement of magnetic energy above the background spectrum. We find this lower limit to be a factor of 10× to 500× higher than what can credibly be attributed to interstellar neutral atoms when the spacecraft is within ~700 R_J of the planet. The per neutral ionization rates that were computed for the previous interstellar source are then combined with the minimum ion production rates that are required to produce observable waves to yield the local neutral H density associated with the wave observations. By integrating over the minimum H^+ production rates and assuming a steady-state population of neutral atoms, we obtain a lower bound for the rate of neutral H atoms lost by the planetary system that reach the solar wind.

Figure 7 shows the computed rate of turbulent transport using Equation 4 for the 98 wave intervals and 56 control intervals studied here. We use the background fits for the total power spectrum that exclude the wave power enhancements as illustrated by the upper red lines in Figure 5. The values of ϵ computed for the wave intervals furthest from Jupiter are consistent with the values for the wave intervals within rarefaction regions arising from newborn interstellar pickup ions (Hollick et al., 2018a, 2018b, 2018c). However, closer to the planet the turbulence rates for wave events are comparable to the rates for the solar wind control intervals and considerably higher

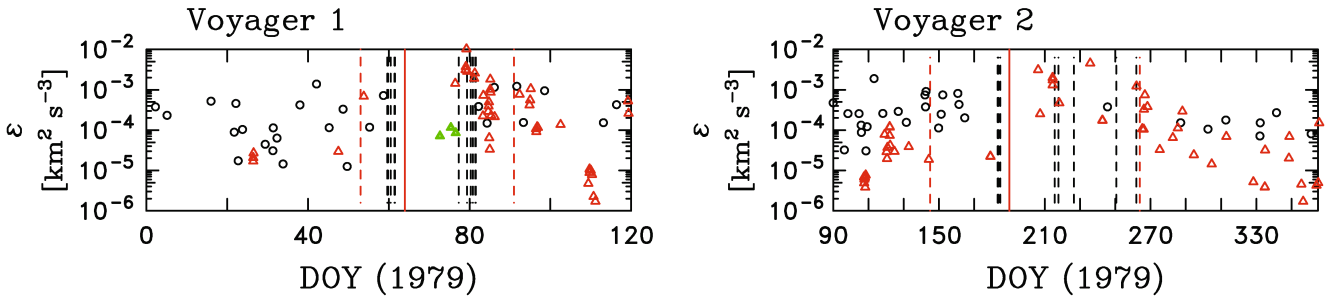

Figure 7. Computed value of turbulent energy cascade rate ϵ.

than observations further from the planet. Waves due to relatively weak pickup sources can only be seen when the background spectral levels are low and the turbulence is weak (Aggarwal et al., 2016; Cannon, Smith, Isenberg, Vasquez, Joyce, et al., 2014; Fisher et al., 2016; Hollick et al., 2018b). Therefore, excitation of waves by newborn interstellar H^+ close to Jupiter is problematic as the turbulence rates are high while the rate of ion production from neutral interstellar atoms is unchanged. The instability due to newborn interstellar H^+ is thereby too weak to produce observed waves within the exclusion intervals as we will demonstrate below.

4.1. Interstellar Neutral Source

The analysis leading to Hollick et al. (2018a) uncovered the wave intervals studied here as part of a search for waves due to newborn interstellar PUIs. In order to rule out interstellar neutral atoms as a possible source for the pickup H^+ that we believe is the source of the waves shown in Figure 5 and analyzed here, we begin by describing our analysis of the interstellar pickup H^+ problem (Hollick et al., 2018b).

The general pickup process for newborn interstellar H^+ begins with a neutral atom moving at ~25 km s^{-1} relative to the Sun (Bzowski et al., 2012, 2015; Gloeckler et al., 1993; McComas et al., 2012, 2015, 2017; Möbius et al., 2012; Schwadron et al., 2015). This velocity represents the motion of the heliosphere through the interstellar medium. The newborn ion's velocity within the rest frame of the solar wind (where the nominal solar wind speed $V_{SW} \sim 450$ km s^{-1}) is converted into cyclotron motion across the local magnetic field and particle streaming along the local magnetic field according to the orientation of the heliospheric magnetic field at the point of ionization. Ionization is accomplished primarily via collision with solar wind protons and photoionization by solar EUV.

The local density of interstellar neutral H was calculated with the use of the numerical Warsaw Test Particle Model (nWTPM) code (Sokół et al., 2015) based on ideas developed by Rucinski and Bzowski (1995, 1996) and Tarnopolski and Bzowski (2009), with the total ionization rates varying with time along the trajectory of atoms and the time-varying latitudinal structure of the solar wind taken into account (according to a model by Sokół et al. [2013]). A more detailed description of the analysis is provided in Hollick et al. (2018b).

Figure 8 (top row) shows the computed rate of H^+ production from interstellar neutral H using nWTPM. Several interesting behaviors are in evidence. The ion production rates for wave intervals tend to be comparable to rates for the local control intervals. This is expected because the in situ magnetic fluctuation levels play no role in ion production. While this equality is expected, the waves arising from the ionization of interstellar H tend to be seen in rarefaction regions despite the fact that in these regions the solar wind flux is low and the ionization rates are comparably low (Cannon, Smith, Isenberg, Vasquez, Joyce, et al., 2014; Hollick et al., 2018b). Observability is not based solely on the rate of ion production, but is most strongly dependent upon the strength of the turbulence that permits the accumulation of wave energy when the turbulence is weak. Ionization rates for interstellar H atoms during some of the Voyager 2 wave events are significantly higher than for the Voyager 1 events. This appears to be within the normal range of temporal variability.

Figure 8 (middle row) shows the resulting rate of wave growth due to newborn interstellar pickup H^+. The derived wave excitation rates for the wave events close to the planet do not appear to be especially higher than for wave events further from the planet or for the local control intervals.

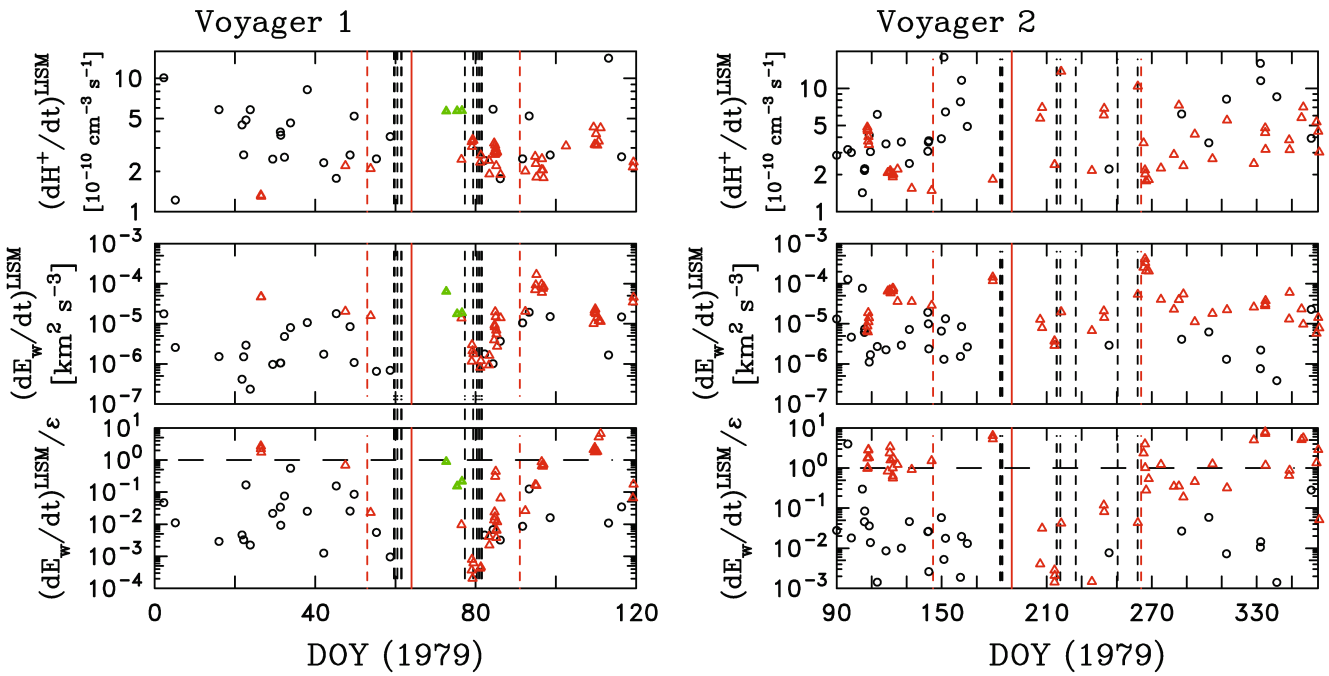

Figure 8. Analysis of intervals based on assumed LISM neutral atom source. (top to bottom) Computed rate of H^+ production from interstellar neutral H, dH^+/dt; resulting growth rate due to H^+ production from interstellar neutral H, $(dE_w/dt)^{LISM}$; and ratio of wave growth rate to turbulent cascade rate $(dE_w/dt)^{LISM}/\epsilon$.

Figure 8 (bottom row) shows the ratio of wave growth rates due to newborn interstellar pickup H^+ and the computed turbulent transport rates obtained by Equation 4. The ratio of $(dE_W/dt)^{LISM}/\epsilon$ is exceptionally low within the exclusion intervals because the magnetic power spectra, and hence the turbulence rates, are higher there. This makes these wave events highly unlikely to arise from an interstellar source.

If the turbulence rates exceed the wave growth rates significantly, the waves should not be seen. Hollick et al. (2018b) applied this idea to Voyager observations from launch through 1990 and found that $(dE_W/dt)/\epsilon > 1$ is a good requirement for wave observations excited by newborn interstellar H^+ unlike waves excited by He^+ that demonstrate a change in the threshold for observation to $(dE_W/dt)/\epsilon > 10^{-1}$ beyond 10 AU. That same work does see a $\pm$ factor of 10 spread about 1 for the H^+ source that is thought to represent either limitations in the turbulence theory used, uncertainties in the power spectrum due to the use of short data intervals, or temporal effects in the turbulence and wave excitation dynamics not included in the analysis. Here we find that wave events within the exclusion intervals have $(dE_W/dt)/\epsilon < 10^{-1}$ and often $<10^{-3}$. Uncertainties for the ion production rate are estimated at a few percent. Other theories for the turbulence may provide different values of ϵ, but the theory employed here provides good agreement with observations at 1 AU (Vasquez et al., 2007) as well as Voyager observations out to ~40 AU (Pine et al., 2020). So even with the uncertainties in the wave excitation and turbulence theories it is unlikely that excitation by interstellar H^+ can overcome a deficit of this magnitude. It does not appear that newborn interstellar H^+ can explain these observations.

4.2. Jovian Neutral H Source

There are no direct measurements for the planetary system outgassing of neutral H atoms on the Voyager spacecraft in the energy range required here, but we can generate estimates for the minimum number density using the wave observations reported here. If the wave growth rate is equated to the turbulence rate $(dE_W/dt) = \epsilon$, a minimum ion production rate can be estimated that is consistent with the observability of the waves. Then, using the per neutral ionization rates already calculated for the interstellar neutrals, we can use the ion production rates to obtain estimates for the local neutral H density.

Figure 9 shows our estimates for the pickup H^+ production rate dH^+/dt obtained via two analyses using the above assumption: The value $(dH^+/dt)^{MIN1}$ is obtained by tracking the wave vector with the fastest growth rate while

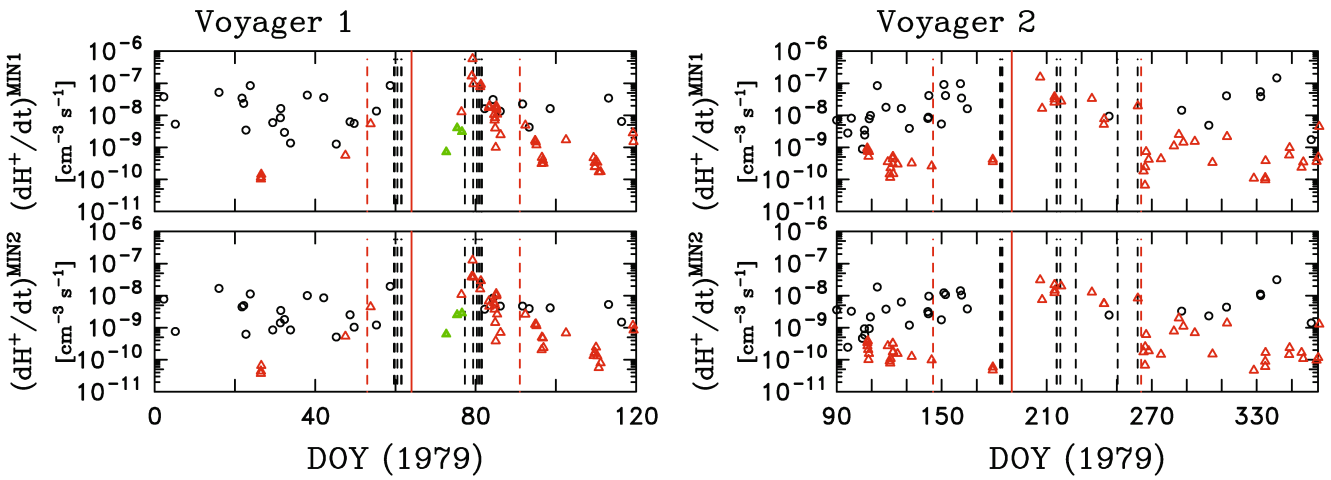

Figure 9. Minimum H^+ production rate obtained by setting $dE_w/dt = \epsilon$. Red and black, solid and dashed vertical lines again represent as above.

$(dH^+/dt)^{MIN2}$ is obtained by tracking the wave vector that shows the greatest wave energy in the analysis of the data. The two analyses are generally in good agreement, but with $(dH^+/dt)^{MIN1} > (dH^+/dt)^{MIN2}$, consistently. The results are tabulated in Tables 3 and 4. Note that wave events outside the exclusion zone tend to show minimum ion production rates in the range of values seen for newborn interstellar PUIs, but inside the exclusion zone the ion rates climb by several orders of magnitude.

Figure 10 replots Figure 9 according to distance from the planet. The vertical dashed lines represent the reported shock crossing times. It is important to understand the shock crossing observations, and the uncertainty in shock crossing times, when interpreting these results. The Voyager 1 outbound shock crossing is at 200 R_J (Bridge et al., 1979a) and Kurth et al. (1981) reports the spacecraft to be in the solar wind from this point onward. Bridge et al. (1979b) reports three outbound shock crossings by Voyager 2 on DOY 215 and a distance of 282.3–283.3 R_J from the planet and they suggest that there may be additional shock crossings at later times. Kurth et al. (1981) argue that there are times after this when Voyager 2 is in magnetospheric plasma which implies shock crossings between DOY 215 and 222 (between 283 and 313 R_J), again between DOYs 222 and 230 (between 313 and 434 R_J), and twice again between DOYs 241 and 263 (541 and 750 R_J). However, no shock crossing times are provided. This introduces considerable uncertainty in the interpretation of the Voyager 2 data as it introduces

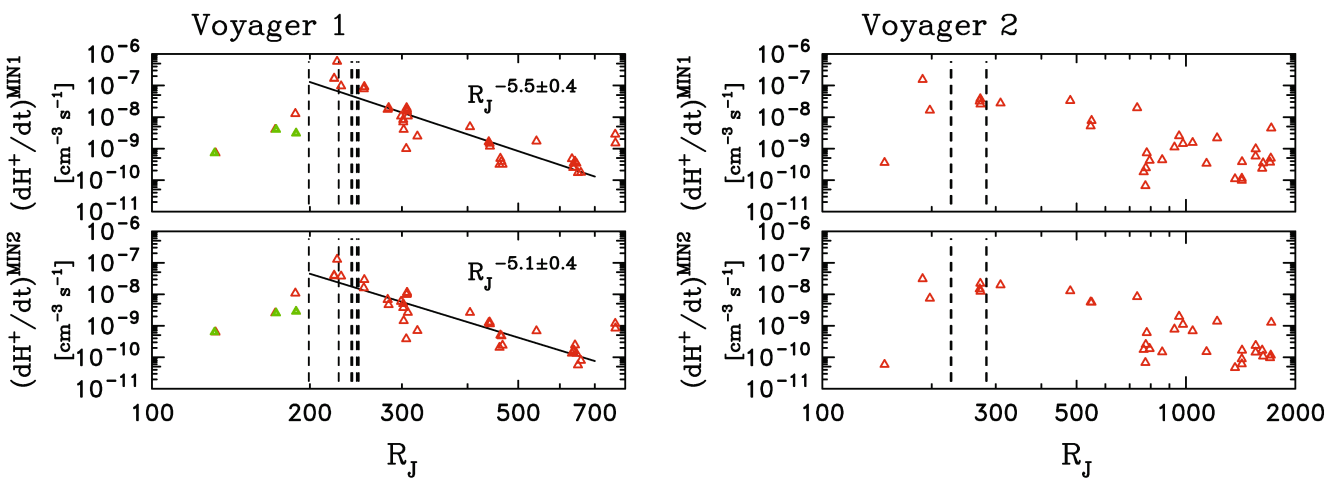

Figure 10. Minimum H^+ production rates obtained by setting $dE_w/dt = \epsilon$ plotted as a function of distance from the planet. We now limit the analysis to only those events seen on the outbound leg of the encounter. The vertical dashed lines represent the outbound crossing of the Jovian bow shock reported by Bridge et al. (1979a, 1979b). Only events with PLS data are used as only these have reliable wave excitation and turbulence rates.

Table 5
Fits to Figure 10 $dH^+/dt = A_{200}^{H^+}(R/200)^n$

S/C	Analysis	$A_{200}^{H^+}$[cm^{-3} s^{-1}]	n
V1	MIN1	$(1.3 \pm 0.4) \times 10^{-7}$	-5.5 ± 0.4
V1	MIN2	$(4.5 \pm 1.4) \times 10^{-8}$	-5.1 ± 0.4

the possibility that some wave events arise from shock-accelerated ions, and it becomes difficult to represent these inferred shock crossings on the plots.

We now focus on the Voyager 1 observations and omit the five events in the event list that are closest to Jupiter, as they are seen inside the bow shock with one located inside the Jovian magnetopause. We also omit the last two wave events in Figure 10 under the assumption that they are likely due to the ionization of interstellar neutrals. The computed minimum rate of pickup ion production for the remaining observations between 200 and 700 R_J is well fit by a power law of the form $dH^+/dt = A_{200}^{H^+}(R/200)^n$. Table 5 lists the fit values for $(dH^+/dt)^{MIN1}$ and $(dH^+/dt)^{MIN2}$ with uncertainties. Note that the exponents are $-5.5 \le n \le -5.1$ which are too steep to be described with uniform expansion of neutral atoms and only minimal depletion by ionization. Either ionization is a major factor in determining the neutral atom density, or there is significant latitudinal dependence for the neutral atom source, or the neutral atoms are accelerating away from the planet, or the source is time-dependent on a time scale of hundreds of days. Note that three of the wave events used in the above fit are seen on the inbound leg of the encounter and have not been reported previously as possible shock-associated wave events.

The Voyager 2 results are more difficult to interpret. Seventeen of the Voyager 2 events shown in Figure 9 and reproduced as a function of distance to Jupiter in Figure 10 are seen on the inbound leg of the encounter with 15 of these events recorded outside the exclusion region. None of the inbound wave events studied here have been interpreted as shock acceleration events (Goldstein et al., 1983, 1984, 1985; Smith & Lee, 1986; Smith et al., 1983, 1984). We also omit one observed wave event that has been attributed to energetic sulfur or oxygen (Goldstein et al., 1986). The most distant inbound event is over 1,000 R_J upstream of the planet and this event is consistent with the interstellar source. Likewise, there are significantly more distant events seen on the outbound leg due to the fact that the spacecraft traveled further down the tail and crossed the shock at a more distant point from Jupiter than did Voyager 1. The folding of distant upstream events with the distant downstream events is potentially problematic as the instability requires time to accumulate the observed wave energy and the outbound observations represent solar wind parcels that have been within the ion cloud for a longer time.

The per neutral ionization rates $\dot{H}$ used to obtain the estimates for newborn interstellar PUI densities can also be used to estimate the number density of neutral H according to $H_{MIN} = (dH^+/dt)^{MIN}/\dot{H}$. Applying this to the MIN1 and MIN2 analyses produces the results shown in Figure 11. What may be most notable in this result is that

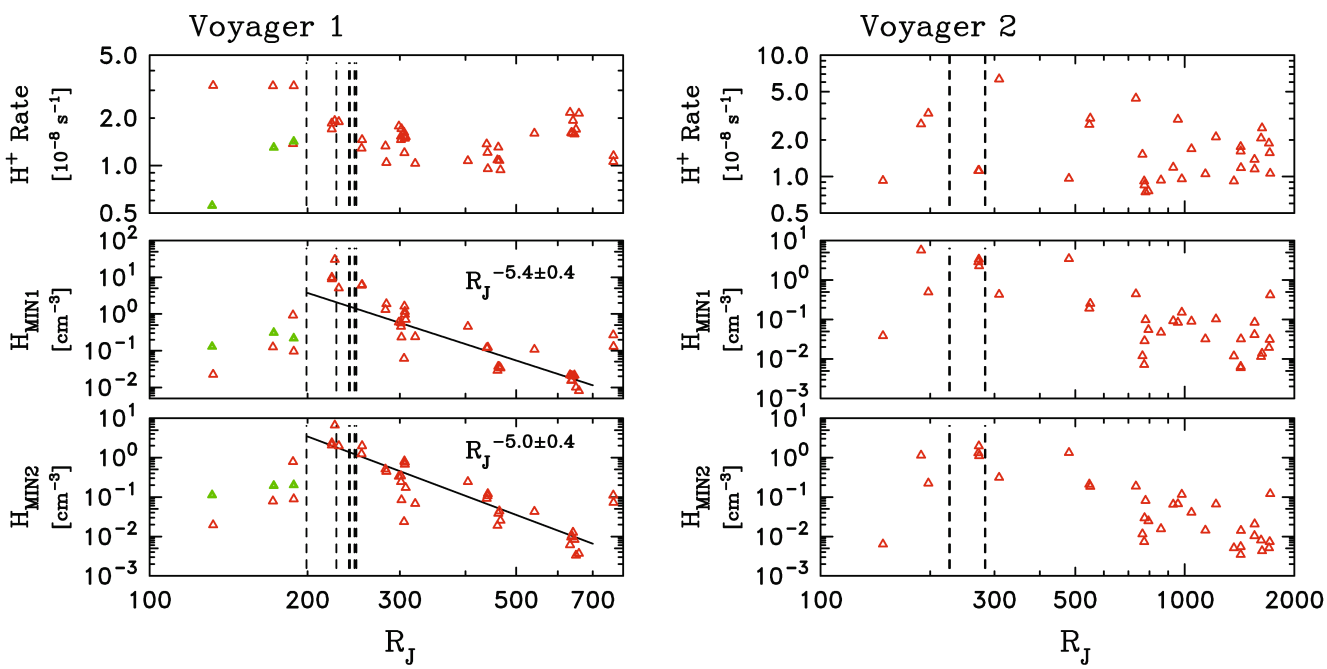

Figure 11. Minimum neutral H density obtained from Figure 10 using the computed per neutral ionization rates described in Hollick et al. (2018b). The vertical dashed line represents the outbound crossing of the Jovian bow shock by Voyager 1.

Table 6
Fits to Figure 11 $H = A_{200}^{H}(R/200)^{n}$

S/C	Analysis	A_{200}^{H} [cm^{-3}s^{-1}]	n
V1	MIN1	8.5 ± 2.7	−5.4 ± 0.4
V1	MIN2	3.0 ± 0.9	−5.0 ± 0.4

the neutral atom density at 200 R_J inferred from the Voyager 1 observations is in the range 3–9 cm^{-3} while the solar wind density is ~0.1 cm^{-3}. The implication is that the solar wind at this time is flowing through a relatively dense cloud of neutral H. We can fit the inferred neutral H densities as a function of distance from the planet according to $H = A_{200}^{H}(R/200)^{n}$. The resulting fit parameters are listed in Table 6.

We can compute the total neutral atom injection rate into the solar wind if we assume a geometry, or spatial extent, for the atoms outside the trajectory of the spacecraft. If we assume that the observed newborn ion density is a population moving with the planet that is otherwise time-independent, then the spatially integrated ion production rate equals the number of neutral atoms injected into the region $R > 200$ R_J. This allows us to estimate the neutral H source rate according to the integrated ion production rates. The fit functions for the newborn ion rates listed in Table 5 can be integrated from 200 to 700 R_J assuming a disk of thickness L in keeping with the general ideas of Mendillo et al. (1990),

$$\left(dH^{+}/dt\right)^{\text{disk}} = 2\pi L(1R_J)^2 A_{200}^{H^+} 200^2 \int_1^{7/2} x^{n+1} dx \tag{5}$$

where 1 $R_J = 7.1 \times 10^7$ cm, both $A_{200}^{H^+}$ and n are given in Table 5, and the upper limit of the integral represents 700 R_J.

To evaluate L, we note that when the waves are observed by Voyager 1 primarily on the outbound leg of the encounter, the spacecraft is 20 R_J above the planet's equatorial plane and approximately the same distance above the plane of the Io and Europa tori. We have no independent assessment of L, but noting the spacecraft location we can consider several possibilities: L = 1, 10, and 40 R_J. The results are listed in Table 7. A disk of thickness L = 10 R_J appears to offer the best agreement with the integrated loss rates based on Cassini observations (Krimigis et al., 2002), but the disk is less space-filling than the spherical assumption of those authors.

We can also compute a neutral H source rate under the assumption that the atoms are ejected from the magnetosphere as a uniform sphere $(dH^{+}/dt)^{\text{sphere}}$ by again using the fit values listed in Table 5. We compute this rate according to:

$$\left(dH^{+}/dt\right)^{\text{sphere}} = 4\pi(1R_J)^3 A_{200}^{H^+} 200^3 \int_1^{7/2} x^{n+2} dx. \tag{6}$$

These results, which are also listed in Table 7, are a factor of 100× higher than those argued by Krimigis et al. (2002) for the same geometry.

We note that the pickup ions that excite the observed waves are so-called "newborn" ions. Wave excitation occurs in association with the scattering process while the asymptotic state of a shell-like distribution of ions is stable. Therefore, it is important that we integrate the ion production rate along the solar wind trajectory and compare the integrated ion density with the solar wind thermal ion density as there is no evidence of deceleration due to mass loading.

Using the fit to the rate of ion production based on minimum values needed to achieve wave growth, we can integrate that function along the path of the solar wind to compute the net accumulation of pickup ions at each point where waves are observed. We derive the expression

$$\int \left(dH^{+}/dt\right) dl = \frac{A_{200}^{H^+}(D/200)^n D \cdot (1R_J)}{V_{SW}} \int_{-90}^{\Theta} \left(\cos\left(\Theta'\right)\right)^{-n} d\Theta' \tag{7}$$

Table 7
Planetary Loss Rate

S/C	Analysis	$(dH^{+}/dt)^{1R_J\text{slab}}$ [s^{-1}]	$(dH^{+}/dt)^{10R_J\text{slab}}$ [s^{-1}]	$(dH^{+}/dt)^{40R_J\text{slab}}$ [s^{-1}]	$(dH^{+}/dt)^{\text{sphere}}$ [s^{-1}]
V1	MIN1	3.3×10^{27}	3.3×10^{28}	1.3×10^{29}	1.9×10^{30}
V1	MIN2	1.3×10^{27}	1.3×10^{28}	5.2×10^{28}	7.7×10^{29}

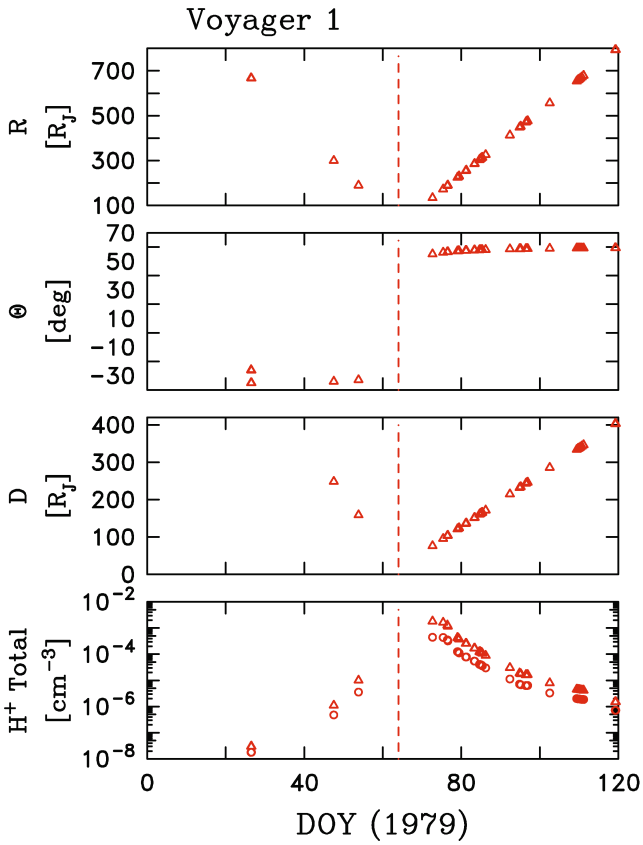

Figure 12. Integrated (total) H^+. The vertical dashed line represents the time of closest approach. Triangles (circles) represent the results of the MIN1 (MIN2) analysis.

where D is the impact parameter (distance of closest approach) for the given parcel of solar wind measured in Jovian radii, V_{SW} is given in units of cm s^{-1}, and Θ is the angle of the spacecraft relative to the dawn meridian ($\Theta = 0°$). Figure 12 shows the resulting total accumulation of pickup H^+ for the wave events along with the distance to Jupiter for each event R. Since the total pickup ion density is significantly less than the solar wind density, there is no concern of significant mass loading by the Jovian pickup ions.

4.3. Shock Acceleration

There remains the question of whether or not the observations reported here could result from particle acceleration by the Jovian bow shock. The nominal characteristics of waves due to shock-accelerated ions are: (1) magnetic connection to the shock, (2) particle spectra that extend above the minimum energy that can reach the upstream region due to multiple encounters with the shock, and (3) wave spectra that extend to frequencies less than the ion cyclotron frequency in the spacecraft frame as a result of the more energetic ions. Fully evolved ion foreshock populations that have scattered onto a spherical distribution are associated with (4) unpolarized wave spectra due to the presence of energetic particles traveling both shockward and anti-shockward along the magnetic field (Lee, 1982; Smith & Lee, 1986). Less evolved, or beam-like, ion populations that have experienced fewer shock collisions may generate polarized wave spectra. We have already shown that the waves do not meet conditions 3 and 4, and by implication the particle populations do not meet condition 2.

We can attempt a direct analysis of condition 1 above using the mean magnetic field direction. We define the standard heliocentric coordinate system ($\hat{R}$, $\hat{T}$, $\hat{N}$) where $\hat{R}$ is directed from the Sun to the spacecraft, $\hat{T}$ is coplanar with the Sun's rotational equator and directed in the sense of rotation, and $\hat{N}$ is given by $\hat{N} = \hat{R} \times \hat{T}$. Figure 13 shows the direction cosine angles of the mean magnetic field during the wave intervals where

$$\Theta_{BR} \equiv \arccos\left(B_R/|B|\right) \tag{8}$$

$$\Theta_{BT} \equiv \arccos\left(B_T/|B|\right) \tag{9}$$

$$\Theta_{BN} \equiv \arccos\left(B_N/|B|\right). \tag{10}$$

These are the angles formed by the mean magnetic field relative to the $\hat{R}$, $\hat{T}$, and $\hat{N}$ directions.

On the inbound trajectory, magnetic connection to the shock is favored by quasiradial mean field directions (Goldstein et al., 1983, 1984, 1985; Smith & Lee, 1986; Smith et al., 1983, 1984). This is what is seen in Figure 13 prior to DOY 60 where the field shows approximate alignment with the inbound trajectory.

On the outbound trajectory, magnetic connection to the shock is favored by $\Theta_{BT} \simeq 0°$ which results in $\Theta_{BR} \simeq \Theta_{BN} \simeq 90°$. Although this is not seen in Figure 13, the data trends weakly in this direction. Inside the shocks, the mean field directions tend toward the radial direction, suggesting a quasi-perpendicular shock geometry for these cases. There are four wave events prior to the first outbound shock crossing when the spacecraft is in the magnetosheath. These events could be interpreted as waves due to shock-accelerated ions excited in the upstream region and then convected through the shock, but they would likely be accelerated by a quasi-perpendicular shock geometry at a very weak shock and this does not favor the acceleration of a significant number of ions or wave excitation. They could also be interpreted as waves due to PUIs of Jovian origin.

Outside the shocks, the mean field directions vary within the $(\hat{T}, \hat{N})$ plane and are generally perpendicular to $\hat{R}$. Figure 3 shows that the outbound trajectory of Voyager 1 takes the spacecraft above the Jovian orbital plane in the $+\hat{N}$ direction. Therefore, when the direction cosine of the mean field is in the $(-\hat{T}, -\hat{N})$ direction, or the $(+\hat{T}, +\hat{N})$ direction, magnetic connection to the shock is unlikely. There are numerous events around DOY 80

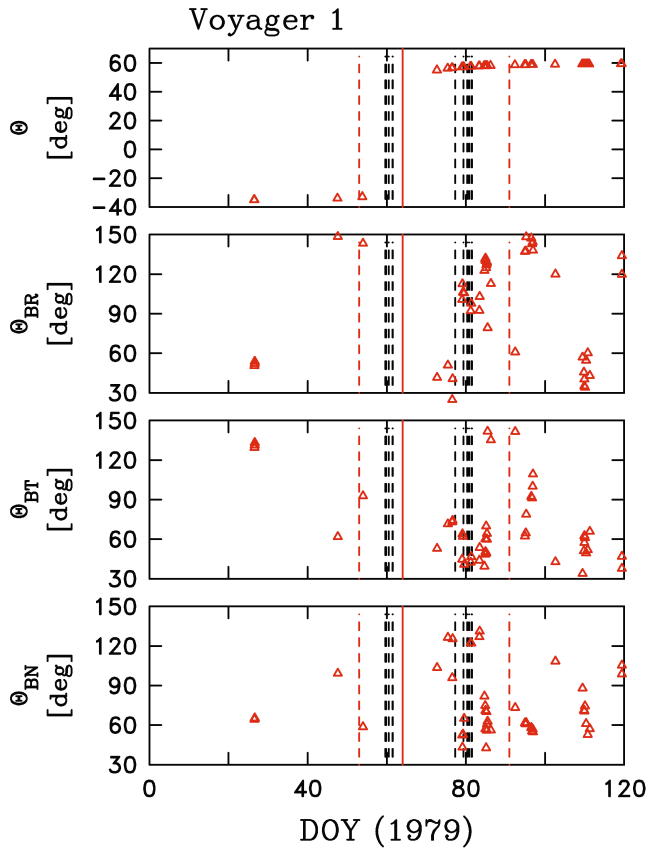

Figure 13. (top to bottom) Angle formed by the spacecraft location relative to the dawn-dusk meridian, and direction cosines angles of the mean magnetic field relative to $(\hat{R}, \hat{T}, \hat{N})$.

in close proximity to the shock. While this suggests an association with the shock, and the local field direction may be of significantly less importance due to the close proximity, there is no evidence in the wave spectra of particle energization beyond the injection energy. From DOY 85 onward the mean field direction tends to be in the $(+\hat{T}, +\hat{N})$ direction which reduces the likelihood of magnetic connection to the shock. At the same time, shock motions are considerable due to oscillations of the plasma torus and these motions propagate down the flanks of the shock making the actual shock crossing times very difficult to compute and beyond the scope of this paper.

We conclude that if the waves observed on the outbound leg arise from energetic H^+ that are accelerated at the shock, then the waves show no evidence of the multiple shock reflections that are required to energize the ions beyond the injection energy. It seems questionable that the shock could perform the initial reflection of solar wind ions into the upstream region, but is unable to provide additional reflections to produce the more energetic population. The absence of wave excitation at $f_{sc} < f_{p,c}$ together with the observed polarization of the waves, would suggest this is the type of shock acceleration present if shock acceleration is responsible for forming the suprathermal ions upstream of the shock. We cannot rule out this possibility, but at this point we are unable to guarantee magnetic connection.

4.4. Magnetospheric Leakage

Leakage of magnetospheric ions through the magnetosheath has been suggested as an alternative to shock acceleration for explaining the energetic particle observations in the upstream region (Anagnostopoulos et al., 1986; Mauk et al., 2019). The suspect ions under this interpretation are generally sulfur or oxygen associated with volcanic activity at Io as their source can be unambiguously identified as Jovian in origin. However, H^+ is argued to be the dominant leaked ion. The analysis presented here does not attempt to discredit the assertion that ions, especially heavy ions may leak from the Jovian magnetosphere. Instead, we note the difficulties in attributing these observed waves to a heavy ion source.

The difficulties in applying this interpretation to the outbound observations shown here are two-fold: First, magnetic connection to the shock is again required as the leaked ion must travel along the magnetic field as it passes through the shock. Second, for the heavy ion population to produce a wave signature at $f_{p,c}$ frequencies and greater, the ion must be traveling through the solar wind at much less than the solar wind speed in order to produce waves at the observed frequency. For those instances where magnetic connection noseward of the spacecraft is implied by the local field, it may be possible to obtain an ion at such a low speed. However, connection too near the nose would require sufficient particle speed to clear the shock which would imply an ion with too much energy to produce the waves seen. The resonant instability requires that the ion move at greater than V_A and nonresonant instabilities generally require greater particle speeds. In an $M_A = 10$ flow, with Oxygen (Sulfur) having an atomic mass of 16 (32), the ion would need to be fully stripped of electrons to possess even marginal instability to resonant processes at these frequencies. The heavy ion source interpretation for these observations is thereby stuck between the need for sufficient energy to reach the observation point, but not so much that it cannot produce the waves at the frequencies seen. We conclude that a leakage interpretation as a direct source of the waves reported here is highly unlikely.

There is one other possible heavy ion source interpretation for these observations and that is that leaked heavy ions may collide with neutral atoms upstream of the shock producing pickup H^+ populations and enhancing the ionization rates used here. This would reduce the number of neutral atoms needed and thereby reduce our estimate for the integrated leakage rate from the Jovian system. This possibility is beyond the scope of the work presented here.

4.5. Thermal Ion Anisotropy

Anisotropies in the thermal ion population tend to exhibit instabilities at these frequencies. However, we have examined the Voyager/PLS data and find no evidence of significant thermal anisotropy in most of the instances when waves are seen and only marginal anisotropy in a few. We conclude that the waves are not excited by anisotropies in the thermal proton population.

5. Discussion

There are no direct measurements of either neutral H or energetic H^+ on the Voyager spacecraft in the energy range of interest here. Therefore, there are no corroborating Voyager measurements to support our interpretation. Cassini/Magnetosphere Imaging Instrument (MIMI) did record an extensive cloud of neutral H extending out 0.5 AU from Jupiter (Krimigis et al., 2002). Singly charged heavy ions are also observed in association with H^+ (Christon et al., 2020). Our inferred extent of the pickup ions that result from the neutral H is 700 $R_J \simeq 0.3$ AU where the limiting consideration is the distance where the inferred Jovian source equals or is less than the background interstellar source. In this respect, there would appear to be an association between the Cassini measurements and the inferred neutral cloud derived from magnetic waves in the Voyager data.

While the analysis presented here cannot pinpoint the source of the inferred neutral H, we do believe that our inferred densities may be associated with observations by the Cassini MIMI Ion Neutral Camera (Krimigis et al., 2004) as reported by Krimigis et al. (2002) and Mauk et al. (2004). That consistency requires that we understand both the abilities and the limitations of the MIMI instrument. Specifically, the Voyager/MAG observations described here require that the neutral H have nearly zero speed relative to the Sun, which means nearly zero speed relative to Jupiter. This assumption derives from the need for the neutral atoms to move through the solar wind at nearly the solar wind speed in order to excite waves at the observed frequency, which means neutral H with an energy of ~1 keV in the solar wind frame. The neutral H energy in the spacecraft frame must be significantly less than 1 keV. Magnetosphere Imaging Instrument measures neutral H in the energy range 5–55 keV. Only if we can extrapolate the MIMI observations down to minimal energy can the MIMI observations be used to limit total neutral H densities in the present analysis. Krimigis et al. (2002) and Mauk et al. (2004) reported neutral H with speeds in the range 10^3–10^4 km s^{-1}. Assuming that the neutral H forms a spherical distribution, they estimate the Jovian loss rate of neutral H to be $(dH/dt)^{\text{sphere}} = 10^{26}$ s^{-1}. They further state that extrapolation to lower energy can easily increase this rate to 10^{27} s^{-1}. It should be noted that Mendillo et al. (1990) derived a disk (rather than sphere) for the extended cloud of neutral sodium. Our analysis suggests that the MIMI measurements may constitute the hot, nonthermal tail of the distribution with a higher core density than extrapolation of the MIMI measurements to low energy would imply. Simulations also suggest that simple extrapolation of the MIMI observations to the particle energies needed here may underestimate the low-energy population (Luhmann, 2003).

It is challenging at present to identify a definitive source for the low-energy neutral H that leads to the pickup H^+ population outside the bow shock. There are simply too many theoretical steps and too many unknowns to connect low-frequency waves in the solar wind to a neutral H source somewhere in the Jovian system. In one possible explanation, Mauk et al. (2003, 2004, 2019) argue that precipitation onto Jupiter can provide a source of energetic neutral H. As an illustration of the uncertainty that exists at this time, Bagenal & Dols (2020) argue that the minimum escape velocity is unlikely to permit Jeans escape from the atmosphere.

Io and Europa both possess neutral clouds and plasma tori at 5.9 and 9.4 R_J (e.g., Broadfoot et al., 1979; Delamere & Bagenal, 2003; Delamere et al., 2004; Mauk et al., 2004; Smyth & Marconi, 2006; Bagenal & Delamere, 2011; Yoshioka et al., 2017; Koga et al., 2018; Smith et al., 2019; Bagenal & Dols, 2020). The Io source is comprised mainly of sulfur and oxygen with no significant hydrogen. The Europa source, however, has an abundant H_2 neutral population with a number density peaking at ~190 cm^{-3} near Europa, dropping to a few cm^{-3} at the opposite side of Jupiter along the moon's orbit (Smith et al., 2019; Smyth & Marconi, 2006). Europa is considered to be the source of the observed energetic neutrals hydrogen atoms that can be produced when electrons or photons interact with H_2 (e.g., Mauk et al., 2004; Smyth & Marconi, 2006). The estimated supply rate of H_2 from Europa is 2×10^{27} H_2/s (Smith et al., 2019; Smyth & Marconi, 2006). Whatever the source of neutral H beyond the bow shock, and the above populations may be candidates for that source, our analysis strongly suggests that only a pickup H^+ population can account for the observed magnetic waves.

In the present analysis, powering the observed wave events via a pickup ion process in the solar wind requires neutral densities of 5 cm^{-3} near 200 R_J and a neutral supply rate greater than 5×10^{28} amu/s. The inferred neutral density decreases rapidly with increasing distance from Jupiter but inside of 200 R_J would need to vary slowly with distance so as to remain consistent with/cws values from current models about the orbit of Europa. The required supply rate is more than an order of magnitude greater than Europa's total hydrogen supply rate. Some 10% of Europa's hydrogen supply is estimated to produce energetic neutral hydrogen atoms and more would be converted to pickup ions close to Europa (Mauk et al., 2004; Smyth & Marconi, 2006). This would leave only a fraction of the total rate available at large distances from the orbit of Europa for further conversion to pickup ions. Thereby, the discrepancy between required and estimated rates is large. As a result, either the source of Europa's neutral atoms is much greater than currently estimated, or a different neutral source is involved, or our estimates of the turbulence rates are too large, or pickup ion processes do not alone account for the bulk of observed wave events.

The magnetic spectra observations reported here are undeniably complex. There are some wave events with signatures extending to $f_{sc} < f_{p,c}$ that are not textbook examples of waves excited by low-energy PUIs. Also, we are unable to explain why the wave source inside the shock is computed to be weaker than the source for waves outside the shock. We have considered shock acceleration, but the field orientations do not favor magnetic connection to the shock. Likewise, excitation by energetic electrons requires magnetic connection that appears to be unavailable and the wave polarizations appear to be in conflict with this source. Energetic neutral atoms seem to be in insufficient number to serve as a source population for the ions. Although challenging, our present interpretation of these waves as arising from a neutral atom source that originates within the Jovian system is the most conservative interpretation we can offer at present.

6. Summary

We have examined a class of magnetic waves observed in the solar wind by the Voyager 1 and 2 spacecraft during the outbound leg of the Jovian encounters. These observations possess all of the expected signatures of waves excited by newborn pickup H^+ with a few exceptions where there does appear to be evidence within the wave spectra of some possible particle acceleration beyond the minimum energy of pickup ion distributions. Our analysis of these observations indicates that they could not result from newborn interstellar pickup H^+ and we are left to conclude that they are most likely associated with a Jovian source. By balancing wave growth against the turbulent processes that destroy the wave signatures and absorb the energy as part of the cascade process that heats the solar wind, we were able to infer minimum pickup ion production rates for the events. These rates were up to a factor 500 higher than the nominal interstellar source. The pickup ion density varied with distance from Jupiter as R^{-5} which is consistent with a Jovian source and neutral atom depletion at greater distances. Once ionized, the pickup particle is convected with the solar wind away from the planet.

The actual ionization processes are the same as those that produce pickup ions from interstellar neutrals. From the ion production rates, we infer a local neutral H density which is as high as 10 cm^{-3} a short distance outside the bow shock at 200 R_J from the planet. When we assume a neutral H population with near-zero motion relative to the planet, we can compare the inferred density to the more energetic H atoms measured by the MIMI instrument on the Cassini spacecraft (Krimigis et al., 2002). Our inferred densities are higher, although our inferred radial extent of the population agrees with the results of these authors. Our estimate of the neutral atom loss rate for the Jovian system varies with the assumed and unmeasured latitudinal extent of the population. Our best estimate places the integrated neutral loss rate at $\sim 5 \times 10^{28}$ s^{-1} with the uncertainty depending primarily on the unknown latitudinal extent of the population.

There are unresolved questions regarding the source of the low-energy neutral H that we argue is present and we cannot answer those questions here. We leave that for future work. Here, we provide a variation on an analysis that has worked well in explaining magnetic field observations that arise from newborn interstellar pickup ions and suggest that the pickup of newly ionized neutrals escaping from the Jovian system represents a likely explanation for the waves observed.

Data Availability Statement

The data used in this study can be obtained at https://cdaweb.gsfc.nasa.gov/.

Acknowledgments
C.W.S., P.A.I., S.H., and Z.B.P. are supported by NASA grant NNX17AB86G. C.W.S., B.J.V., P.A.I., A.S.W., and A.V.M. are supported by NASA HSR Grant 80NSSC18K1215. C.W.S., B.J.V., P.A.I., and N.A.S. were partially supported by NASA Grant 80NSSC17K0009. B.J.V. is supported by NASA Grant 80NSSC19K0832. C.J.J. and N.A.S. are supported by the Interstellar Boundary Explorer mission as a part of NASAs Explorer Program, partially by NASA SR&T Grant NNG06GD55G, and the Sun-2-Ice (NSF Grant No. AGS1135432) project. M.B. and M.A.K. acknowledge the support by the Polish National Science Center Grant 2015/19/B/ST9/01328. The data used in this analysis are available from the NSSDC. The authors wish to thank N. F. Ness and L. F. Burlaga of the MAG team as well as the PLS team for providing the data used in this study.

References

Adhikari, L., Zank, G. P., Bruno, R., Telloni, D., Hunana, P., Dosch, A., et al. (2015a). The transport of low-frequency turbulence in astrophysical flows. II. Solutions for the super-Alfvénic solar wind. *Journal of Physics: Conference Series*, *642*, 012001. https://doi.org/10.1088/1742-6596/642/1/012001

Adhikari, L., Zank, G. P., Bruno, R., Telloni, D., Hunana, P., Dosch, A., et al. (2015b). The transport of low-frequency turbulence in the super-Alfvénic solar wind. *The Astrophysical Journal*, *805*(1), 63. https://doi.org/10.1088/0004-637x/805/1/63

Adhikari, L., Zank, G. P., Hunana, P., Shiota, D., Bruno, R., Hu, Q., & Telloni, D. (2017). II. Transport of nearly incompressible magnetohydrodynamic turbulence from 1 to 75 au. *The Astrophysical Journal*, *841*(2), 85. https://doi.org/10.3847/1538-4357/aa6f5d

Aggarwal, P., Taylor, D. K., Smith, C. W., Joyce, C. J., Fisher, M. K., Isenberg, P. A., et al. (2016). Voyager observations of magnetic waves due to newborn interstellar pickup ions: 2–6 au. *The Astrophysical Journal*, *822*(2), 94. https://doi.org/10.3847/0004-637x/822/2/94

Anagnostopoulos, G. C., Sarris, E. T., & Krimigis, S. M. (1986). Quasi-periodic behavior of ion events and wave activity upstream from Jupiter's bow shock: Ulysses' observations. *Journal of Geophysical Research*, *91*(A3), 3020–3028. https://doi.org/10.1029/ja091ia03p03020

Argall, M. R., Hollick, S. J., Pine, Z. B., Smith, C. W., Joyce, C. J., Isenberg, P. A., et al. (2017). Observation of magnetic waves excited by newborn interstellar pickup He+ observed by the Voyager 2 spacecraft at 30 au. *The Astrophysical Journal*, *849*(1), 61. https://doi.org/10.3847/1538-4357/aa8ee2

Argall, M. R., Hollick, S. J., Pine, Z. B., Smith, C. W., Joyce, C. J., Isenberg, P. A., et al. (2018). Erratum: "Observation of magnetic waves excited by newborn interstellar pickup He+ observed by the Voyager 2 spacecraft at 30 au. *The Astrophysical Journal*, *854*(1), 77. https://doi.org/10.3847/1538-4357/aaab5c

Bagenal, F., Adriani, A., Allegrini, F., Bolton, S. J., Bonfond, B., Bunce, E. J., et al. (2017). Magnetospheric science objectives of the Juno mission. *Space Science Reviews*, *213*(1–4), 219–287. https://doi.org/10.1007/s11214-014-0036-8

Bagenal, F., & Delamere, P. A. (2011). Flow of mass and energy in the magnetospheres of Jupiter and Saturn. *Journal of Geophysical Research*, *116*(A5), A05209. https://doi.org/10.1029/2010JA016294

Bagenal, F., & Dols, V. (2020). The space environment of Io and Europa. *Journal of Geophysical Research*, *125*(5), e2019JA027485. https://doi.org/10.1029/2019JA027485

Bamert, K., Kallenbach, R., Ness, N. F., Smith, C. W., Terasawa, T., Hilchenbach, M., et al. (2004). Hydromagnetic wave excitation upstream of an interplanetary traveling shock. *The Astrophysical Journal Letters*, *601*(1), L99–L102. https://doi.org/10.1086/381962

Belcher, J. W., & Davis, L., Jr. (1971). Large-Amplitude Alfvén waves in the interplanetary medium, 2. *Journal of Geophysical Research*, *76*(16), 3534–3563. https://doi.org/10.1029/ja076i016p03534

Bieber, J. W., Wanner, W., & Matthaeus, W. H. (1996). Dominant two-dimensional solar wind turbulence with implications for cosmic ray transport. *Journal of Geophysical Research*, *101*(A2), 2511–2522. https://doi.org/10.1029/95ja02588

Breech, B., Cranmer, S. R., Matthaeus, W. H., Kasper, J. C., & Oughton, S. (2010). Heating of the solar wind with electron and proton effects. In *Paper presented at 12th International Solar Wind Conference* (pp. 214–217).

Breech, B., Matthaeus, W. H., Cranmer, S. R., Kasper, J. C., & Oughton, S. (2009). Electron and proton heating by solar wind turbulence. *Journal of Geophysical Research*, *114*(A9), A09103. https://doi.org/10.1029/2009ja014354

Breech, B., Matthaeus, W. H., Minnie, J., Bieber, J. W., Oughton, S., Smith, C. W., & Isenberg, P. A. (2008). Turbulence transport throughout the heliosphere. *Journal of Geophysical Research*, *113*(A8), A08105. https://doi.org/10.1029/2007ja012711

Breech, B., Matthaeus, W. H., Minnie, J., Oughton, S., Parhi, S., Bieber, J. W., & Bavassano, B. (2005). Radial evolution of cross helicity in high latitude solar wind. *Geophysical Research Letters*, *32*(6), L06103. https://doi.org/10.1029/2004gl022321

Bridge, H. S., Belcher, J. W., Butler, R. J., Lazarus, A. J., Mavretic, A. M., Sullivan, J. D., et al. (1977). The plasma experiment on the 1977 Voyager mission. *Space Science Reviews*, *21*(3), 259–287. https://doi.org/10.1007/bf00211542

Bridge, H. S., Belcher, J. W., Lazarus, A. J., Sullivan, J. D., McNutt, R. L., Bagenal, F., et al. (1979a). Plasma observations near Jupiter: Initial results from Voyager 1. *Science*, *204*(4396), 987–991. https://doi.org/10.1126/science.204.4396.987

Bridge, H. S., Belcher, J. W., Lazarus, A. J., Sullivan, J. D., McNutt, R. L., Bagenal, F., et al. (1979b). Plasma observations near Jupiter: Initial results from Voyager 2. *Science*, *206*(4421), 972–976. https://doi.org/10.1126/science.206.4421.972

Broadfoot, A. L., Belton, M. J. S., Takacs, P. Z., Sandel, B. R., Shemansky, D. E., Holberg, J. B., et al. (1979). Extreme ultraviolet observations from Vogayer 1 encounter with Jupiter. *Science*, *204*(4396), 979–982. https://doi.org/10.1126/science.204.4396.979

Bzowski, M., Kubiak, M. A., Möbius, E., Bochsler, P., Leonard, T., Heirtzler, D., et al. (2012). Neutral interstellar helium parameters based on IBEX-Lo observations and test particle calculations. *The Astrophysical Journal Supplement Series*, *198*(2), 12. https://doi.org/10.1088/0067-0049/198/2/12

Bzowski, M., Swaczyna, P., Kubiak, M. A., Sokol, J. M., Fuselier, S. A., Galli, A., et al. (2015). Interstellar neutral helium in the heliosphere from IBEX observations. III. Mach number of flow, velocity vector, and temperature from the first six years of measurements. *The Astrophysical Journal Supplement Series*, *220*(2), 28. https://doi.org/10.1088/0067-0049/220/2/28

Cannon, B. E., Smith, C. W., Isenberg, P. A., Vasquez, B. J., Joyce, C. J., Murphy, N., & Nuno, R. G. (2014). Ulysses observations of magnetic waves due to newborn interstellar pickup ions. 2. Application of turbulence concepts to limiting wave energy and observability. *The Astrophysical Journal*, *787*, 133. https://doi.org/10.1088/0004-637x/787/2/133

Cannon, B. E., Smith, C. W., Isenberg, P. A., Vasquez, B. J., Murphy, N., & Nuno, R. G. (2014). Ulysses observations of magnetic waves due to newborn interstellar pickup ions. 1. New observations and linear analysis. *The Astrophysical Journal*, *784*(2), 150. https://doi.org/10.1088/0004-637x/784/2/150

Christon, S. P., Hamilton, D. C., Mitchell, D. G., Plane, J. M. C., & Nylund, S. R. (2020). Suprathermal magnetospheric atomic and molecular heavy ions at and near Earth, Jupiter, and Saturn: Observations and identification. *Journal of Geophysical Research*, *125*(1), e2019JA027271. https://doi.org/10.1029/2019ja027271

Dasso, S., Milano, L. J., Matthaeus, W. H., & Smith, C. W. (2005). Anisotropy in fast and slow solar wind fluctuations. *The Astrophysical Journal Letters*, *635*(2), L181–L184. https://doi.org/10.1086/499559

Delamere, P. A., & Bagenal, F. (2003). Modeling variability of plasma conditions in the Io torus. *Journal of Geophysical Research*, *108*(A7), A071276. https://doi.org/10.1029/2002JA009706

Delamere, P. A., Steffl, A., & Bagenal, F. (2004). Modeling temporal variability of plasma conditions in the Io torus during the Cassini era. *Journal of Geophysical Research*, *109*(A10), A10216. https://doi.org/10.1029/2003JA010354

Fisher, M. K., Argall, M. R., Joyce, C. J., Smith, C. W., Isenberg, P. A., Vasquez, B. J., et al. (2016). A survey of magnetic waves excited by newborn interstellar He^{+} observed by the ACE spacecraft at 1 au. *The Astrophysical Journal*, *830*, 47. https://doi.org/10.3847/0004-637x/830/1/47

Fowler, R. A., Kotick, B. J., & Elliott, R. D. (1967). Polarization analysis of natural and artificially induced geomagnetic micropulsations. *Journal of Geophysical Research*, *72*(11), 2871–2883. https://doi.org/10.1029/jz072i011p02871

Gloeckler, G., Galvin, A. B., Ipavich, F. M., Geiss, J., Balsiger, H., von Steiger, R., et al. (1993). Detection of interstellar pickup hydrogen in the solar system. *Science*, *261*(5117), 70–73. https://doi.org/10.1126/science.261.5117.70

Goldstein, M. L., Smith, C. W., & Matthaeus, W. H. (1983). Large-amplitude MHD waves upstream of the Jovian bow shock. *Journal of Geophysical Research*, *88*(A12), 9989–9999. https://doi.org/10.1029/ja088ia12p09989

Goldstein, M. L., Smith, C. W., & Matthaeus, W. H. (1984). Correction to "Large-amplitude MHD waves upstream of the Jovian bow shock". *Journal of Geophysical Research*, *89*(A10), 9161. https://doi.org/10.1029/ja089ia10p09161

Goldstein, M. L., Wong, H. K., & Eviatar, A. (1986). Excitation of MHD waves upstream of Jupiter by energetic sulfur or oxygen ions. *Journal of Geophysical Research*, *91*(A7), 7954–7960. https://doi.org/10.1029/ja091ia07p07954

Goldstein, M. L., Wong, H. K., Viñas, A. F., & Smith, C. W. (1985). Large-amplitude MHD waves upstream of the Jovian bow shock: Reinterpretation. *Journal of Geophysical Research*, *90*(A1), 302–310. https://doi.org/10.1029/ja090ia01p00302

Gosling, J. T., & Skoug, R. M. (2002). On the origin of radial magnetic fields in the heliosphere. *Journal of Geophysical Research*, *107*(A10), 1327. https://doi.org/10.1029/2002ja009434

Hamilton, K., Smith, C. W., Vasquez, B. J., & Leamon, R. J. (2008). Anisotropies and helicities in the solar wind inertial and dissipation ranges at 1 AU. *Journal of Geophysical Research*, *113*(A1), A01106. https://doi.org/10.1029/2007ja012559

Hollick, S. J., Smith, C. W., Pine, Z. B., Argall, M. R., Joyce, C. J., Isenberg, P. A., et al. (2018a). Magnetic waves excited by newborn interstellar pickup ions measured by the Voyager spacecraft from 1 to 45 au. I. Wave properties. *The Astrophysical Journal*, *263*, 75. https://doi.org/10.3847/1538-4357/aac83b

Hollick, S. J., Smith, C. W., Pine, Z. B., Argall, M. R., Joyce, C. J., Isenberg, P. A., et al. (2018b). Magnetic waves excited by newborn interstellar pickup ions measured by the Voyager spacecraft from 1 to 45 au. II. Instability and turbulence analyses. *The Astrophysical Journal*, *263*, 76. https://doi.org/10.3847/1538-4357/aac839

Hollick, S. J., Smith, C. W., Pine, Z. B., Argall, M. R., Joyce, C. J., Isenberg, P. A., et al. (2018c). Magnetic waves excited by newborn interstellar pickup ions measured by the Voyager spacecraft from 1 to 45 au. III. Observation times. *The Astrophysical Journal Supplement Series*, *237*(2), 34. https://doi.org/10.3847/1538-4365/aac83a

Isenberg, P. A. (2005). Turbulence-driven solar wind heating and energization of pickup protons in the outer heliosphere. *The Astrophysical Journal*, *623*(1), 502–510. https://doi.org/10.1086/428609

Isenberg, P. A., Smith, C. W., & Matthaeus, W. H. (2003). Turbulent heating of the distant solar wind by interstellar pickup protons. *The Astrophysical Journal*, *592*(1), 564–573. https://doi.org/10.1086/375584

Isenberg, P. A., Smith, C. W., Matthaeus, W. H., & Richardson, J. D. (2010). Turbulent heating of the distant solar wind by interstellar pickup protons in a decelerating flow. *The Astrophysical Journal*, *719*(1), 716–721. https://doi.org/10.1088/0004-637x/719/1/716

Joyce, C. J., Smith, C. W., Isenberg, P. A., Murphy, N., & Schwadron, N. A. (2010). Excitation of low-frequency waves in the solar wind by newborn interstellar pickup ions H^+ and He^+ as seen by Voyager at 4.5 AU. *The Astrophysical Journal*, *724*(2), 1256–1261. https://doi.org/10.1088/0004-637x/724/2/1256

Kennel, C. F., Coroniti, F. V., Scarf, F. L., Livesey, W. A., Russell, C. T., Smith, E. J., et al. (1986). A test of Lee's quasi-linear theory of ion acceleration by interplanetary traveling shocks. *Journal of Geophysical Research*, *91*(A11), 11917–11928. https://doi.org/10.1029/ja091ia11p11917

Kirsch, E., Krimigis, S. M., Kohl, J. W., & Keath, E. P. (1981). Upper limits for X-ray and energetic neutral particle emission from Jupiter: Voyager-1 results. *Geophysical Research Letters*, *8*(2), 169–172. https://doi.org/10.1029/gl008i002p00169

Koga, R., Tsuchiya, F., Kagitani, M., Sakanoi, T., Yoneda, M., Yoshioka, K., et al. (2018). Spatial distribution of Io's oxygen cloud observed by Hisaki. *Journal of Geophysical Research*, *123*(5), 3764–3776. https://doi.org/10.1029/2018JA025328

Kolmogorov, A. N. (1941). The local structure of turbulence in incompressible viscous fluid for very large Reynolds numbers. *Doklady Akademii Nauk SSSR*, *30*, 301–305. (Reprinted in Proceedings of the Royal Society London A, 434, 9–13, 1991).

Krimigis, S. M., Mitchell, D. G., Hamilton, D. C., Dandouras, J., Armstrong, T. P., Bolton, S. J., et al. (2002). A nebula of gases from Io surrounding Jupiter. *Nature*, *415*(6875), 994–996. https://doi.org/10.1038/415994a

Krimigis, S. M., Mitchell, D. G., Hamilton, D. C., Livi, S., Danduras, J., Jaskulek, S., et al. (2004). Magnetosphere Imaging Instrument (MIMI) on the Cassini mission to Saturn/Titan. *Space Science Reviews*, *114*(1–4), 233–329. https://doi.org/10.1007/s11214-004-1410-8

Kurth, W. S., Gurnett, D. A., Scarf, F. L., Poynter, R. L., & Sullivan, J. D. (1981). Voyager observations of Jupiter's distant magnetotail. *Journal of Geophysical Research*, *86*(A10), 8402–8412. https://doi.org/10.1029/ja086ia10p08402

Leamon, R. J., Smith, C. W., Ness, N. F., Matthaeus, W. H., & Wong, H. K. (1998). Observational constraints on the dynamics of the interplanetary magnetic field dissipation range. *Journal of Geophysical Research*, *103*(A3), 4775–4787. https://doi.org/10.1029/97ja03394

Leamon, R. J., Smith, C. W., Ness, N. F., & Wong, H. K. (1999). Dissipation range dynamics: Kinetic Alfvén waves and the importance of β_e. *Journal of Geophysical Research*, *104*(A10), 22331–22344. https://doi.org/10.1029/1999ja900158

Lee, M. A. (1982). Coupled hydromagnetic wave excitation and ion acceleration upstream of the Earth's bow shock. *Journal of Geophysical Research*, *87*(A7), 5063–5080. https://doi.org/10.1029/ja087ia07p05063

Lee, M. A. (1983). Coupled hydromagnetic wave excitation and ion acceleration upstream of interplanetary travelling shocks. *Journal of Geophysical Research*, *88*(A8), 6109–6119. https://doi.org/10.1029/ja088ia08p06109

Lee, M. A., & Ip, W.-H. (1987). Hydromagnetic wave excitation by ionized interstellar hydrogen and helium in the solar wind. *Journal of Geophysical Research*, *92*(A10), 11041–11052. https://doi.org/10.1029/ja092ia10p11041

Lepping, R. P., Burlaga, L. F., Klein, L. W., Jessena, J. M., & Goodrich, C. C. (1981). Observations of the magnetic field and plasma flow in Jupiter's magnetosheath. *Journal of Geophysical Research*, *86*(A10), 8141–8155. https://doi.org/10.1029/ja086ia10p08141

Luhmann, J. G. (2003). Expected heliospheric attributes of Jovian pickup ions from the extended neutral gas disk. *Planetary and Space Science*, *51*(6), 387–392. https://doi.org/10.1016/s0032-0633(03)00034-5

Marchuk, A. V., Smith, C. W., Watson, A. S., Argall, M. R., Isenberg, P. A., Vasquez, B. J., et al. (2021). Low-frequency waves due to newborn interstellar pickup He^+ observed by the Ulysses spacecraft. *The Astrophysical Journal*, *923*(2), 185. https://doi.org/10.3847/1538-4357/ac2eb3

Matthaeus, W. H., & Goldstein, M. L. (1982). Measurement of the rugged invariants of magnetohydrodynamic turbulence in the solar wind. *Journal of Geophysical Research*, *87*(A8), 6011–6028. https://doi.org/10.1029/ja087ia08p06011

Matthaeus, W. H., Goldstein, M. L., & Roberts, D. A. (1990). Evidence for the presence of quasi-two-dimensional nearly incompressible fluctuations in the solar wind. *Journal of Geophysical Research*, *95*(A12), 20673–20683. https://doi.org/10.1029/ja095ia12p20673

Matthaeus, W. H., Oughton, S., Pontius, D. H., Jr., & Zhou, Y. (1994). Evolution of energy containing turbulent eddies in the solar wind. *Journal of Geophysical Research*, *99*(A10), 19267–19287. https://doi.org/10.1029/94ja01233

Matthaeus, W. H., & Velli, M. (2011). Who needs turbulence? *Space Science Reviews*, *160*(1–4), 145–168. https://doi.org/10.1007/s11214-011-9793-9

Matthaeus, W. H., & Zhou, Y. (1989). Extended inertial range phenomenology of magnetohydrodynamic turbulence. *Physics of Fluids B*, *1*(9), 1929–1931. https://doi.org/10.1063/1.859110

Mauk, B. H., Cohen, I. J., Haggerty, D. K., Hospodarsky, G. B., Connerney, J. E. P., Anderson, B. J., et al. (2019). Investigation of mass-/charge-dependent escape of energetic ions across the magnetopauses of Earth and Jupiter. *Journal of Geophysical Research*, *124*(7), 5539–5567. https://doi.org/10.1029/2019ja026626

Mauk, B. H., Mitchell, D. G., Krimigis, S. M., Roelof, E. C., & Paranicas, C. P. (2003). Energetic neutral atoms from a trans-Europa gas torus at Jupiter. *Nature*, *421*(6926), 920–922. https://doi.org/10.1038/nature01431

Mauk, B. H., Mitchell, D. G., McEntire, R. W., Paranicas, C. P., Roelof, E. C., Williams, D. J., et al. (2004). Energetic ion characteristics and neutral gas interactions in Jupiter's magnetosphere. *Journal of Geophysical Research*, *109*(A9), 9. https://doi.org/10.1029/2003ja010270

McComas, D. J., Alexashov, D., Bzowski, M., Fahr, H., Heerikhuisen, J., Izmodenov, V., et al. (2012). The heliosphere's interstellar interaction: No bow shock. *Science*, *336*(6086), 1291–1293. https://doi.org/10.1126/science.1221054

McComas, D. J., Bzowski, M., Fuselier, S. A., Frisch, P. C., Galli, A., Izmodenov, V. V., et al. (2015). Local interstellar medium: Six years of direct sampling by IBEX. *The Astrophysical Journal Supplement Series*, *220*(2), 22. https://doi.org/10.1088/0067-0049/220/2/22

McComas, D. J., Zirnstein, E. J., Bzowski, M., Elliott, H. A., Randol, B., Schwadron, N. A., et al. (2017). Seven years of imaging the global heliosphere with IBEX. *The Astrophysical Journal Supplement Series*, *233*(1), 8. https://doi.org/10.3847/1538-4365/aa91d2

Means, J. D. (1972). Use of the three-dimensional covariance matrix in analyzing the polarization properties of plane waves. *Journal of Geophysical Research*, *77*(28), 5551–5559. https://doi.org/10.1029/ja077i028p05551

Mendillo, M., Baumgardner, J., Flynn, B., & Hughes, W. J. (1990). The extended sodium nebula of Jupiter. *Nature*, *348*(6299), 312–314. https://doi.org/10.1038/348312a0

Mish, W. H., Wenger, R. M., Behannon, K. W., & Byrnes, J. B. (1982). *Interactive digital signal processor*. *NASA Technical Memorandum 83997*. Goddard Space Flight Center. (Revised 1984).

Möbius, E., Bochsler, P., Bzowski, M., Heirtzler, D., Kubiak, M. A., Kucharek, H., et al. (2012). Interstellar gas flow parameters derived from Interstellar Boundary Explorer-Lo observations in 2009 and 2010: Analytic analysis. *The Astrophysical Journal Supplement Series*, *198*(2), 11. https://doi.org/10.1088/0067-0049/198/2/11

Montagud-Camps, V., Grappin, R., & Verdini, A. (2018). Turbulent heating between 0.2 and 1 au: A numerical study. *The Astrophysical Journal*, *853*(2), 153. https://doi.org/10.3847/1538-4357/aaa1ea

Murphy, N., Smith, E. J., & Schwadron, N. A. (2002). Strongly underwound magnetic fields in co-rotating rarefaction regions: Observations and implications. *Geophysical Research Letters*, *29*(22), 2066–23-4. https://doi.org/10.1029/2002gl015164

Ness, N. F., Acuña, M. H., Lepping, R. P., Burlaga, L. F., Behannon, K. W., & Neubauer, F. M. (1979a). Magnetic field studies at Jupiter by Voyager 1: Preliminary results. *Science*, *204*(4396), 982–987. https://doi.org/10.1126/science.204.4396.982

Ness, N. F., Acuña, M. H., Lepping, R. P., Burlaga, L. F., Behannon, K. W., & Neubauer, F. M. (1979b). Magnetic field studies at Jupiter by Voyager 2: Preliminary results. *Science*, *206*(4421), 966–972. https://doi.org/10.1126/science.206.4421.966

Ng, C. S., Bhattacharjee, A., Munsi, D., Isenberg, P. A., & Smith, C. W. (2010). Kolmogorov versus Iroshnikov-Kraichnan spectra: Consequences for ion heating in the solar wind. *Journal of Geophysical Research*, *115*(A2), A02101. https://doi.org/10.1029/2009ja014377

Oughton, S., Dmitruk, P., & Matthaeus, W. H. (2006). A two-component phenomenology for homogeneous magnetohydrodynamic turbulence. *Physics of Plasmas*, *13*(4), 042306. https://doi.org/10.1063/1.2188088

Oughton, S., Matthaeus, W. H., Smith, C. W., Breech, B., & Isenberg, P. A. (2011). Transport of solar wind fluctuations: A two-component model. *Journal of Geophysical Research*, *116*(A8), A08105. https://doi.org/10.1029/2010ja016365

Parker, E. N. (1963). *Interplanetary dynamical processes*. Wiley-Interscience.

Pine, Z. B., Smith, C. W., Hollick, S. J., Argall, M. R., Vasquez, B. J., Isenberg, P. A., et al. (2020). Solar wind turbulence from 1 to 45 au. IV. Turbulent transport and heating of the solar wind using Voyager observations. *The Astrophysical Journal*, *900*(2), 94. https://doi.org/10.3847/1538-4357/abab12

Rankin, D., & Kurtz, R. (1970). Statistical study of micropulsation polarizations. *Journal of Geophysical Research*, *75*(28), 5444–5458. https://doi.org/10.1029/ja075i028p05444

Richardson, J. D. (2002). The magnetosheaths of the outer planets. *Planetary and Space Science*, *50*(5–6), 503–517. https://doi.org/10.1016/s0032-0633(02)00029-6

Richardson, J. D., Paularena, K. I., Lazarus, A. J., & Belcher, J. W. (1995). Evidence of a solar wind slowdown in the outer heliosphere? *Geophysical Research Letters*, *22*(12), 1469–1472. https://doi.org/10.1029/95gl01421

Richardson, J. D., Phillips, J. L., Smith, C. W., & Gray, P. C. (1996). Thermal anisotropies in the solar wind: Evidence of heating by interstellar pickup ions? *Geophysical Research Letters*, *23*(22), 3259–3262. https://doi.org/10.1029/96gl02909

Richardson, J. D., & Smith, C. W. (2003). The radial temperature profile of the solar wind. *Geophysical Research Letters*, *30*(5), 1206. https://doi.org/10.1029/2002gl016551

Rucinski, D., & Bzowski, M. (1995). Modulation of interplanetary hydrogen distribution during the solar cycle. *Astronomy and Astrophysics*, *296*, 248–263.

Rucinski, D., & Bzowski, M. (1996). Ionization processes in the solar wind—Rates and methods of their determination. *Space Science Reviews*, *78*(1), 265–276. https://doi.org/10.1007/bf00170813

Schwadron, N. A. (2002). An explanation for strongly underwound magnetic field in co-rotating rarefaction regions and its relationship to footpoint motion on the Sun. *Geophysical Research Letters*, *29*(14), 8-1–8-4. https://doi.org/10.1029/2002gl015028

Schwadron, N. A., & McComas, D. J. (2005). The sub-Parker spiral structure of the heliospheric magnetic field. *Geophysical Research Letters*, *32*(3), L03112. https://doi.org/10.1029/2004gl021579

Schwadron, N. A., Möbius, E., Leonard, T., Fuselier, S. A., McComas, D. J., Heirtzler, D., et al. (2015). Determination of interstellar He parameters using five years of data form the IBEX: Beyond closed form approximations. *The Astrophysical Journal Supplement Series*, *220*(2), 25. https://doi.org/10.1088/0067-0049/220/2/25

Smith, C. W. (1989). Anisotropy of shock accelerated ion distributions in interplanetary space. *Journal of Geophysical Research*, *94*(A5), 5474–5478. https://doi.org/10.1029/ja094ia05p05474

Smith, C. W. (2009). Turbulence in space plasmas. In C. J. Schrijver & G. Siscoe (Eds.), *Chapter 7 in Heliophysics I. Plasma Physics of the Local Cosmos*. Cambridge University Press.

Smith, C. W., Goldstein, M. L., & Matthaeus, W. H. (1983). Turbulence analysis of the Jovian upstream 'wave' phenomenon. *Journal of Geophysical Research*, *88*(A7), 5581–5593. https://doi.org/10.1029/ja088ia07p05581

Smith, C. W., Goldstein, M. L., Matthaeus, W. H., & Vinas, A. F. (1984). Correction to "Turbulence analysis of the Jovian upstream 'wave' phenomenon". *Journal of Geophysical Research*, *89*(A10), 9159–9160. https://doi.org/10.1029/ja089ia10p09159

Smith, C. W., Isenberg, P. A., Matthaeus, W. H., & Richardson, J. D. (2006). Turbulent heating of the solar wind by newborn interstellar pickup protons. *The Astrophysical Journal*, *638*(1), 508–517. https://doi.org/10.1086/498671

Smith, C. W., & Lee, M. A. (1986). Coupled hydromagnetic wave excitation and ion acceleration upstream of the Jovian bow shock. *Journal of Geophysical Research*, *91*(A1), 81–90. https://doi.org/10.1029/ja091ia01p00081

Smith, C. W., Matthaeus, W. H., Zank, G. P., Ness, N. F., Oughton, S., & Richardson, J. D. (2001). Heating of the low-latitude solar wind by dissipation of turbulent magnetic fluctuations. *Journal of Geophysical Research*, *106*(A5), 8253–8272. https://doi.org/10.1029/2000ja000366

Smith, C. W., Vasquez, B. J., & Stemkowski, M. R. (2013). Analysis of multi-dimensional correlation functions in the solar wind. *AIP Conference Proceedings*, *1539*, 271–274.

Smith, H. T., Mitchell, D. G., Johnson, R. E., Mauk, B. H., & Smith, J. E. (2019). Europa neutral torus confirmation and characterization based on observations and modeling. *The Astrophysical Journal*, *871*(1), 69. https://doi.org/10.3847/1538-4357/aaed38

Smyth, W. H., & Marconi, M. L. (2006). Europa's atmosphere, gas tori, and magnetospheric implications. *Icarus*, *181*(2), 510–525. https://doi.org/10.1016/j.icarus.2005.10.019

Sokół, J. M., Bzowski, M., Tokumaru, M., Fujiki, K., & McComas, D. J. (2013). Heliolatitude and time variations of solar wind structure from in situ measurements and interplanetary scintillation observations. *Solar Physics*, *285*(1–2), 167–200. https://doi.org/10.1007/s11207-012-9993-9

Sokół, J. M., Kubiak, M. A., Bzowski, M., & Swaczyna, P. (2015). Interstellar neutral helium in the heliosphere from IBEX observations. II. The Warsaw Test Particle Model (WTPM). *The Astrophysical Journal Supplement Series*, *220*(2), 27. https://doi.org/10.1088/0067-0049/220/2/27

Tarnopolski, S., & Bzowski, M. (2009). Neutral interstellar hydrogen in the inner heliosphere under the influence of wavelength-dependent solar radiation pressure. *Astronomy and Astrophysics*, *493*(1), 207–216. https://doi.org/10.1051/0004-6361:20077058

Usmanov, A. V., Goldstein, M. L., & Matthaeus, W. H. (2012). Three-dimensional magnetohydrodynamic modeling of the solar wind including pickup protons and turbulence transport. *The Astrophysical Journal*, *754*(1), 40. https://doi.org/10.1088/0004-637x/754/1/40

Usmanov, A. V., Goldstein, M. L., & Matthaeus, W. H. (2014). Three-fluid, three-dimensional magnetohydrodynamic solar wind model with eddy viscosity and turbulent resistivity. *The Astrophysical Journal*, *788*(1), 43. https://doi.org/10.1088/0004-637x/788/1/43

Usmanov, A. V., Goldstein, M. L., & Matthaeus, W. H. (2016). A four-fluid MHD model of the solar wind/interstellar medium interaction with turbulence transport and pickup protons as separate fluid. *The Astrophysical Journal*, *820*(1), 17. https://doi.org/10.3847/0004-637x/820/1/17

Vasquez, B. J., Smith, C. W., Hamilton, K., MacBride, B. T., & Leamon, R. J. (2007). Evaluation of the turbulent energy cascade rates from the upper inertial range in the solar wind at 1 AU. *Journal of Geophysical Research*, *112*(A7), A07101. https://doi.org/10.1029/2007ja012305

Williams, L. L., & Zank, G. P. (1994). Effect of magnetic field geometry on the wave signature of the pickup of interstellar neutrals. *Journal of Geophysical Research*, *99*(A10), 19229–19244. https://doi.org/10.1029/94ja01657

Williams, L. L., Zank, G. P., & Matthaeus, W. H. (1995). Dissipation of pickup-induced waves: A solar wind temperature increase in the outer heliosphere? *Journal of Geophysical Research*, *100*(A9), 17059–17067. https://doi.org/10.1029/95ja01261

Yoshioka, K., Tsuchiya, F., Kimura, T., Kagitani, M., Murakami, G., Yamazaki, A., et al. (2017). Radial variation of sulfur and oxygen ions in the Io plasma torus as deduced from remote observations by Hisaki. *Journal of Geophysical Research*, *122*(3), 2999–3012. https://doi.org/10.1002/2016JA023691

Zank, G. P., Adhikari, L., Hunana, P., Shiota, D., Bruno, R., & Telloni, D. (2017). Theory and transport of nearly incompressible magnetohydrodynamic turbulence. *The Astrophysical Journal*, *835*(2), 147. https://doi.org/10.3847/1538-4357/835/2/147

Zank, G. P., Dosch, A., Hunana, P., Florinski, V., Matthaeus, W. H., & Webb, & G. M. (2012). The transport of low-frequency turbulence in astrophysical flows. I. Governing equations. *The Astrophysical Journal*, *745*(1), 35. https://doi.org/10.1088/0004-637x/745/1/35

Zank, G. P., Matthaeus, W. H., & Smith, C. W. (1996). Evolution of turbulent magnetic fluctuation power with heliospheric distance. *Journal of Geophysical Research*, *101*(A8), 17093–17107. https://doi.org/10.1029/96ja01275

Zhou, Y., & Matthaeus, W. H. (1990a). Remarks on transport theories of interplanetary fluctuations. *Journal of Geophysical Research*, *95*(A9), 14881–14892. https://doi.org/10.1029/ja095ia09p14863

Zhou, Y., & Matthaeus, W. H. (1990b). Transport and turbulence modeling of solar wind fluctuations. *Journal of Geophysical Research*, *95*(A7), 10291–10311. https://doi.org/10.1029/ja095ia07p10291